Evaluation and optimization of seismic networks and algorithms for earthquake early warning – the case of Istanbul (Turkey)

Adrien Oth,[1] Maren Böse,[2] Friedemann Wenzel,[3] Nina Köhler,[3,5] and Mustafa Erdik[4]

Received 4 February 2010; revised 1 June 2010; accepted 2 July 2010; published 28 October 2010.

[1] Earthquake early warning (EEW) systems should provide reliable warnings as quickly as possible with a minimum number of false and missed alarms. Using the example of the megacity Istanbul and based on a set of simulated scenario earthquakes, we present a novel approach for evaluating and optimizing seismic networks for EEW, in particular in regions with a scarce number of instrumentally recorded earthquakes. We show that, while the current station locations of the existing Istanbul EEW system are well chosen, its performance can be enhanced by modifying the parameters governing the declaration of warnings. Furthermore, unless using ocean bottom seismometers or modifying the current EEW algorithm, additional stations might not lead to any significant performance increase.

Citation: Oth, A., M. Böse, F. Wenzel, N. Köhler, and M. Erdik (2010), Evaluation and optimization of seismic networks and algorithms for earthquake early warning – the case of Istanbul (Turkey), *J. Geophys. Res.*, *115*, B10311, doi:10.1029/2010JB007447.

1. Introduction

[2] Earthquake early warning (EEW) represents an important tool for seismic risk mitigation, since it fills the gap between long-term hazard assessment [e.g., *Petersen et al.*, 2008] and postevent rapid response tools [*Wald et al.*, 2003], allowing for preventive action such as defining appropriate building codes, and facilitating efficient search and rescue operations, respectively. In between these, EEW systems operate during the co-seismic stage of an earthquake by providing short-term (in the order of a few to several tens of seconds) warnings of impending strong ground shaking at a given user site, for instance a heavily populated metropolitan area.

[3] The usefulness of EEW systems, however, strongly depends on their ability to provide both fast and reliable warnings. As a general rule, there is a trade-off between these two requirements [*Böse et al.*, 2008]. Providing warnings more quickly leads to a loss of accuracy due to the smaller amount of seismological information available, whereas, for the same reason, a higher degree of reliability involves a loss of warning time.

[4] Several algorithms for tackling the EEW problem exist [*Kanamori*, 2005; *Allen et al.*, 2009b]. The types of information they provide can differ: while the EEW systems operational in, e.g., Mexico [*Espinosa-Aranda et al.*, 1995] and Istanbul [*Erdik et al.*, 2003] provide rather qualitative warnings (basically stating whether strong ground motion is expected or not), others like the one recently implemented by the Japan Meteorological Agency [*Kamigaichi et al.*, 2009] or those currently undergoing real-time testing in California [*Allen et al.*, 2009a; *Böse et al.*, 2009; *Cua et al.*, 2009] provide quantitative regional ground motion estimates (for instance of peak ground velocity), resulting in so-called alert maps. No matter which methodology is chosen, the implementation of an EEW system requires either the existence of a seismic network not specifically designed for EEW (which may, therefore, be supplemented by a given number of sensors) or the design of an entirely new network. Furthermore, each EEW methodology involves automated rules to decide if a warning shall be issued or not. These rules need a certain number of system parameters that have to be set appropriately.

[5] Efficient EEW aiming at both fast and accurate warnings thus requires an optimally designed seismic network (or supplementation of an existing one) and the best set of algorithm parameters. Optimum network design is not straightforward, since it strongly depends on the seismotectonic setting of the region of interest, funding availability (which directly translates into sensor and infrastructure availability), and other constraints. These requirements might also differ for different EEW algorithms.

[6] Designing EEW systems thus requires systematic evaluation and optimization. While significant advances have been made in understanding the general feasibility and limitations of EEW algorithms [*Allen et al.*, 2009b, and references therein] and communication technology [*Böse et al.*, 2009], little attention has been paid to optimization so far. In order to contribute to this need, we developed a

[1]European Center for Geodynamics and Seismology, Walferdange, Grand-Duchy of Luxembourg.
[2]Seismological Laboratory, California Institute of Technology, Pasadena, California, USA.
[3]Geophysical Institute, Karlsruhe Institute of Technology (KIT), Karlsruhe, Germany.
[4]Kandilli Observatory and Earthquake Research Institute, Department of Earthquake Engineering, Bogazici University, Istanbul, Turkey.
[5]Now at Swiss Re Europe S.A., Niederlassung Deutschland, Unterföhring, Germany.

0148-0227/10/2010JB007447

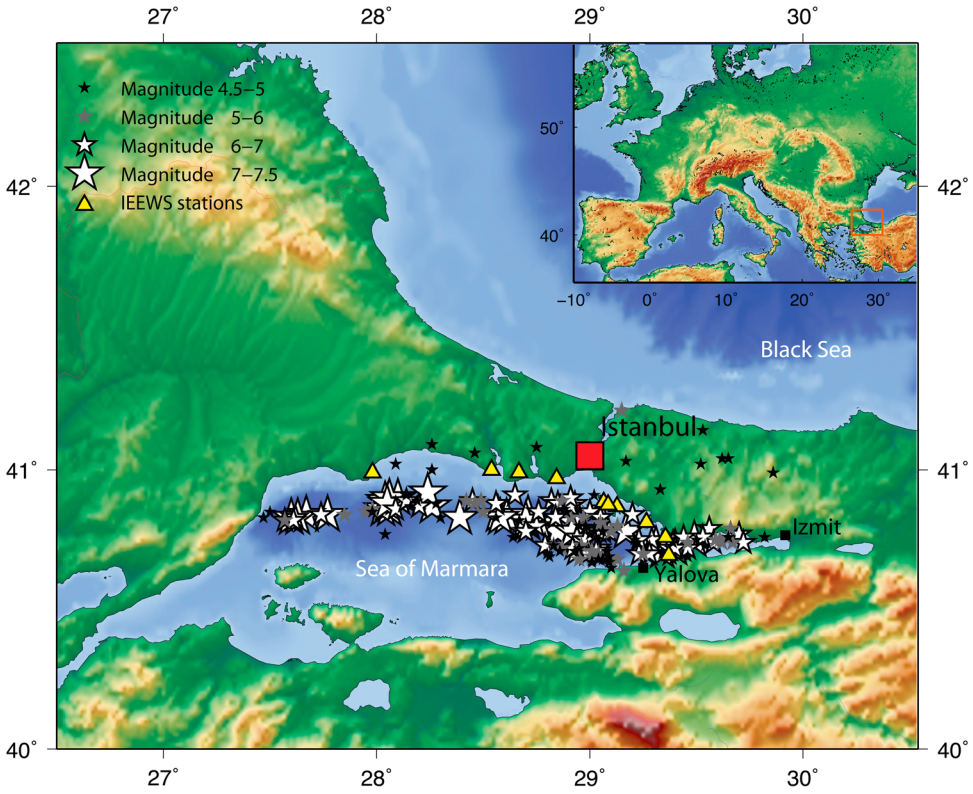

Figure 1. Epicenters of the 180 simulated scenario earthquakes in the Marmara region around Istanbul. 150 events are simulated along five fault segments in the Sea of Marmara (see Figure 3a) and 30 are randomly distributed around the city. This set of scenario earthquakes covers a wide range of potential seismic events in the Sea of Marmara region and is used to evaluate the performance of different EEW systems. The ten stations of the current Istanbul EEW system (IEEWS) are shown as yellow triangles (three of them located on the Prince's Islands southeast of Istanbul), and the user site for warnings, downtown Istanbul, is marked with a red square.

systematic optimization technique for EEW systems, and we demonstrate this approach on the example of the Istanbul EEW system. Starting with the evaluation of the current Istanbul EEW system, we then investigate the effect of changes in the algorithm parameters currently used in the system and finalize our discussion by optimizing the seismic network design using a microgenetic algorithm and a cost function designed to compare the performance of different EEW system variants.

2. The Current Istanbul Earthquake Early Warning System (IEEWS)

[7] The seismic risk in Istanbul is considerable [*Hubert-Ferrari et al.*, 2000] caused by its proximity to the North Anatolian fault below the Sea of Marmara [*Armijo et al.*, 2002; *Le Pichon et al.*, 2002] and its dense population. The probability for an earthquake of magnitude 7 or larger beneath the Sea of Marmara in the time span 2004–2034 has been calculated to be 35%–70% [*Parsons*, 2004]. In response to this threat, the Istanbul EEW system (IEEWS) was installed in 2002 [*Erdik et al.*, 2003]. The IEEWS comprises ten real-time 3-component accelerometric sensors distributed along the shoreline of the Sea of Marmara (Figure 1). The current system is based on three trigger thresholds that need to be exceeded at three or more sensors within 5 seconds before a warning is declared. The current thresholds are 0.02, 0.05, and 0.1 g, corresponding to warning classes I, II, and III, respectively [*Erdik et al.*, 2003]. The trigger thresholds need to be large enough to avoid false alarms caused by small earthquakes and small enough to provide reliable warnings for moderate to large events with strong shaking, without missing important alarms. The current values have been chosen based on expert judgment, without a clear quantitative relationship to the expected ground motions in Istanbul.

3. Finite Fault Stochastic Seismogram Simulation

[8] Our optimization approach requires recordings of earthquakes that are representative for the seismic activity in the given region, including both small and large magnitude earthquakes on all potentially active faults. Alike in most regions in the world, respective data in the Marmara region is very sparse, and therefore the simulation of synthetic seismograms from sets of scenario earthquakes is unavoidable.

[9] In order to assess the performance of the IEEWS, we therefore constructed a massive database of 36,000 synthetic seismograms from 150 scenario earthquakes (Figures 1 and 2) along five fault segments beneath the Sea of

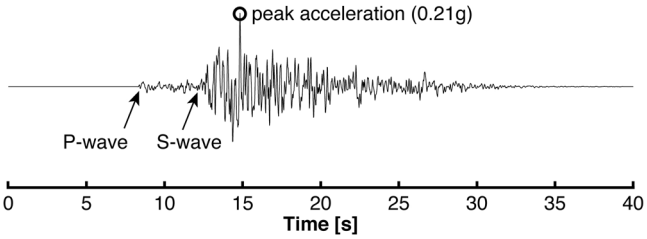

Figure 2. Example for a simulated acceleration time history in Istanbul from a magnitude 6.9 earthquake with an epicentral distance of 33 km. Shown are the typical features of interest in EEW, the *P*- and *S*-wave onsets, as well as the peak ground motion.

Marmara (Figure 3a) [*Böse et al.*, 2008] with moment magnitudes ranging from 4.5 to 7.5 using the extended finite-fault stochastic simulation technique (FFSST) for seismic *P*- and *S*-wave motion [*Beresnev and Atkinson*, 1997; *Böse*, 2006; *Böse et al.*, 2008]. Additionally, 30 randomly distributed events with magnitudes between 4.5 and 5.0 were considered. Seismograms were calculated on a grid of potential station locations with 0.1° grid spacing in latitude and longitude surrounding Istanbul (128 onshore and 112 offshore sites; Figure 3a), as well as at the selected user site for warnings, downtown Istanbul. The 112 offshore locations within the Sea of Marmara were considered as potential sites of ocean bottom seismometers (OBS).

[10] The FFSST divides the fault plane of an earthquake into a number of subfaults, each of which is assumed to

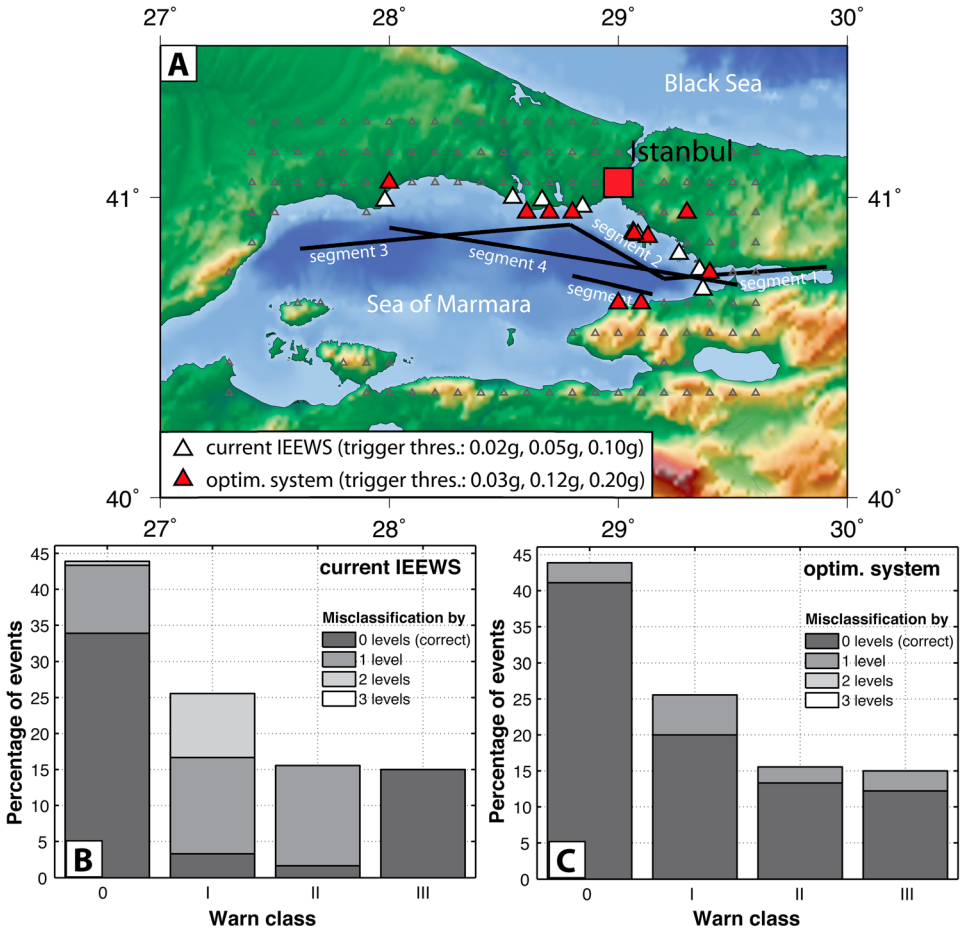

Figure 3. (a) Comparison of sensor locations of the current Istanbul EEW system (IEEWS) and optimized system with ten sensors. The grey open triangles represent the grid of potential onshore station locations at which synthetic seismograms are generated from all scenario earthquakes. Three grid points were included on the Prince's Islands southeast of Istanbul, exactly co-located with the current stations. The five segments on which the set of scenario earthquakes were simulated are shown as black lines. Segment 4 represents joint ruptures of segment 1, 2, and 3. (b) Classification errors for the current IEEWS. Each bar shows the percentage of events of the respective class (0-III) in the simulated set of earthquakes. The different gray scales indicate how many of the events within a given class have been correctly classified (darkest), or have been under-estimated or overestimated by one, two or three levels, respectively. Note the large amount of misclassified events of class I (especially those misclassified by two levels) and II. These events are overestimated to be class III, i.e., highly damaging, earthquakes. (c) Same as (b) for the optimized system of ten stations. Note the strong increase of correctly classified earthquakes.

behave as a point source radiating seismic waves. For each of these subfaults, the ground motion at the observation site is calculated using appropriate models for the velocity structure, source spectral shape, and geometrical and anelastic attenuation [*Böse*, 2006; *Böse et al.*, 2008]. Site amplification effects were estimated from the topographic slope that can be considered as a rough proxy for the shear wave velocity of the uppermost 30 m, V_{S30} [*Wald and Allen*, 2007]. The corresponding data were downloaded from the global V_{S30} map server provided by the United States Geological Survey at 30 arc-sec resolution (http://earthquake.usgs.gov/vs30/). From the V_{S30} estimates, each potential station location was assigned to one of the National Earthquake Hazard Reduction Program (NEHRP) site classes and an average site amplification function (considering linear soil behavior) for the respective class was used [*Boore and Joyner*, 1997]. Even though this approach provides first order estimates of site amplification only and considerable deviations might exist from this average amplification at a given site, it is at present the best approach to include a systematic estimate of site effects in ground motion simulations at a large number of sites. Of course, if empirical site response studies or borehole data were available, they could also be used to characterize site response at these locations. Most grid points were associated with NEHRP C site response class, only few of them as NEHRP B or D. For the grid of potential OBS locations beneath the Sea of Marmara, the topography-based approach cannot be used and we considered these grid points as NEHRP C sites.

[11] The final seismogram from a given earthquake at a given site is obtained by a summation of the contributions from the different subfaults with appropriate time lags to account for the rupture propagation and different lengths of subfault-receiver paths, and appropriate weights corresponding to the (variable) radiation strength of each subfault, accounting for the typically observed slip heterogeneity [*Somerville et al.*, 1999]. Amplitude levels as well as frequency content and duration of ground motion were calibrated with observations from the Izmit and Düzce earthquakes and from a small event (M 4.3) which occurred in the Sea of Marmara, as well as to agree with typical ground motion attenuation relationships [*Böse*, 2006]. The slip distributions on the fault were randomly generated. Both the random phase of the stochastic procedure and the slip distribution have significant impact on the generated time histories. Therefore, we obtain somewhat different warning times for different realizations. Considering in this study a large dataset of different scenario events, we assume to give a reasonable reflection of the aleatory variability of any (large) set of recorded ground motions.

[12] The synthetic seismograms were not perturbed through adding noise to the traces. Visual inspection of accelerometric data recorded by the surface sensor of the Ataköy vertical array located in the western part of Istanbul [*Parolai et al.*, 2009] not very far away from one of the current IEEWS stations show for instance a time domain noise level of the order of 0.1 mg, which is two orders of magnitude lower than the lowest trigger threshold we are considering (0.01 g). Therefore, seismic noise should not have a serious impact on the discrimination between small and large events based on time domain trigger threshold exceedance.

[13] As a representation of the current IEEWS, the grid nodes closest to the current sensor locations were picked. Since in the current IEEWS methodology, time domain amplitude information of the entire seismograms, rather than phase information of the early *P*-wave signals is being used, stochastically simulated ground motions calibrated to realistic amplitude levels are suitable synthetic data in this case.

4. Optimization Approach

[14] With the database described above, we have now at hand a set of scenario earthquakes for which an EEW system for Istanbul should show the best possible performance. As mentioned at the beginning of the previous section, it is of highest relevance that these scenario earthquakes cover all faults around Istanbul that might be capable of generating earthquakes posing a hazard to the city. If this were not the case, the optimally designed EEW system would not be able to appropriately deal with events occurring in these unconsidered source regions, which in turn could lead to missing important alarms. In the case of Istanbul, the seismic hazard is practically entirely determined by the branches of the North Anatolian fault beneath the Sea of Marmara, which are, according to current knowledge, the only structures in the immediate vicinity of Istanbul that can support such large earthquakes. Therefore, by defining a set of scenario events providing a detailed coverage of these potential source regions throughout the entirety of the Sea of Marmara, we are confident not to have forgotten any relevant source zone for the Istanbul EEW system. The 30 randomly distributed smaller scenario events account for the possibility that a smaller earthquake might also occur off the North Anatolian fault as well.

[15] The optimization results presented in this article depend of course on the dataset of simulated seismograms used for this purpose. Due to the large number of parameters involved in the calculation of the latter and limited computational resources, it is impossible to provide a detailed analysis of the impact of each of these parameters on the final optimization results. However, tests using subsets of the database led to stable results very similar to those obtained using the full dataset, which are described below.

[16] Once this set of representative scenario earthquakes is defined, there are three cases that should be considered.

4.1. Performance Evaluation of An Existing EEW System

[17] If sensors are in place and the algorithm and its parameters specified, then the system performance of an EEW system can be evaluated for a set of scenario events. First attempts of such a performance evaluation have recently been made in southern Italy [*Zollo et al.*, 2009], with a particular interest in finite-fault effects.

[18] For a proper evaluation of the IEEWS, it is necessary to provide a quantitative relationship between ground motion in Istanbul (user site for warnings) and each warning class. Therefore, we considered earthquakes causing peak ground acceleration (PGA) in Istanbul of $0.02\ g \leq PGA < 0.07\ g$ as class I events (i.e., for these events, a class I warning should be declared), with $0.07\ g \leq PGA < 0.12\ g$ as class II, and with $PGA \geq 0.12\ g$ as class III events. For this

classification, we followed the rule of thumb that ground motions with PGA > ~0.1 g are considered as potentially seriously damaging [*Anderson*, 2003], and with our choice, class I and II each cover a range of 0.05 g. Earthquakes with PGA < 0.02 g are considered as class 0 events, i.e., no warning should be declared. Note that these class definition thresholds simply determine what warning class should be declared by the EEW system for a given event in the optimal case, and they are different from the trigger thresholds of the EEW system (which determine what warning class is really declared by the considered system). The choice of these class definition thresholds is to some degree arbitrary and should be adapted to the desired system sensitivity or users' needs if known. Note that for an event of warning class III, class I and II alarms will be declared first.

[19] For each simulated scenario earthquake, the available warning time for a given class is calculated as the difference between the time when the class definition threshold in Istanbul is first exceeded (e.g., for class II when the ground motion in Istanbul first exceeds 0.07 g) and the time when the trigger threshold of that class has been exceeded at three sensors within 5 seconds (e.g., for the current IEEWS, 0.05 g for class II).

[20] The evaluation of the performance of the current system can then be done by considering the available warning times for all scenario earthquakes as well as the number of correctly and incorrectly classified events. Whether or not the performance of the system is considered acceptable depends on the criteria set by the user of the system. Concerning the current IEEWS, as mentioned earlier, the current trigger thresholds are set to 0.02, 0.05, and 0.1 g, corresponding to warning classes I, II, and III, respectively [*Erdik et al.*, 2003], and these are smaller than the chosen class definition thresholds in Istanbul in our case. Hence, as the sensors of the current system are of course closer to the fault segments beneath the Sea of Marmara than downtown Istanbul and since obviously ground motion amplitudes decrease with increasing distance, it can be expected that with these class definition thresholds in Istanbul, the current system might provide a relatively large number of false alarms, as we show later. Therefore, we expect that the trigger thresholds would need to be increased for the current system in order to increase its performance with the used definition of warning classes.

4.2. Evaluation and Optimization of EEW Algorithm Parameters (Here: Trigger Thresholds)

[21] The parameters of an EEW algorithm can be evaluated and optimized by applying the algorithm to the set of scenario events under the variation of the parameters. What makes this step nontrivial is the fact that, as soon as different variants of the EEW system are compared with each other, it is necessary to define an appropriate cost function (or objective function), whose value for a given EEW system variant depends both on the available warning times and classification performance (taking into account also the effects of false and missed alarms) for all scenario events.

[22] Using the cost function described in the following section, we performed a systematic search over different trigger threshold combinations while keeping the sensor locations of the current IEEWS fixed in order to find the lowest cost combination of the trigger thresholds.

4.3. Evaluation and Optimization of a Seismic Network

[23] The evaluation and optimization of a new seismic network is the most challenging task and involves either supplementing an existing network with additional sensors or designing a completely new network. It requires the determination of both optimal locations for the (additional) sensors and the best system parameters at the same time. Depending on their number, the parameters may be optimized by simple search over different combinations of them; however, this becomes difficult (if not impossible) if sensor locations have to be also optimized at the same time, because for the latter usually a large number of possible solutions exist. For this reason and because this problem cannot be formulated as a simple linear inverse problem, nonlinear optimization techniques such as simulated annealing or genetic algorithms come into play.

5. Cost Function and Microgenetic Algorithm

5.1. The Cost Function

[24] In every optimization problem, the choice of the cost function is most essential for evaluating the quality of a given set of model parameters. A model performing best considering one cost function may not remain to be the best when considering another one. The definition of an appropriate cost function is not straightforward in this case because we are not fitting synthetic data calculated with a set of model parameters to observations in the classical sense [*Tarantola*, 2005]. Instead, we need a cost function that is able to find the EEW system configuration with largest warning times at the highest level of reliability (i.e., best classification performance). Since there is usually a trade-off between these two requirements [*Böse et al.*, 2008], the cost function has to find the best compromise between them.

[25] Furthermore, a class II event, e.g., should be characterized by two warning times, one for class I and one for class II, because the exceedance of the higher trigger threshold requires also the exceedance of the threshold of the lower class. In the case of erroneous classification as class I event, no warning time of class II is available that could be evaluated. Instead, the effect of the missed alarm of class II has to be accounted for in the cost function. A similar problem arises in the case of false alarms, i.e., if the warning class declared is too high.

[26] We have developed a cost function to cope with these problems:

$$\text{cost} = \sum_{i=1}^{N_{evt}} W_i \left[L \cdot (1-K) \cdot sigmoid(t_{warn,i}, t_{center}, S) + K \right] \quad (1)$$

with

$$sigmoid(t_{warn,i}, t_{center}, S) = 1 - \frac{1}{1 + \exp\left[-S(t_{warn,i} - t_{center})\right]}. \quad (2)$$

$t_{warn,i}$ represents the available warning time for the ith event, and t_{center} is a fixed center time of the sigmoid function, i.e., the time where the sigmoid function takes the value 1/2. The sigmoid in (2) equals one for $t_{warn} \ll t_{center}$ (small,

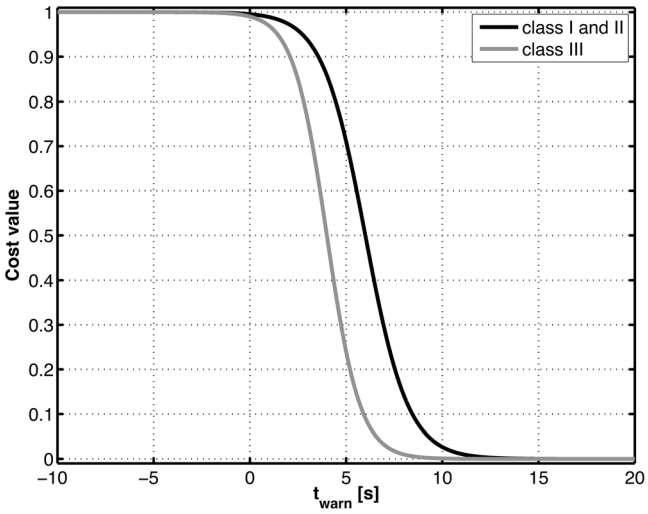

Figure 4. Sigmoid function as defined in equation (2) for the evaluation of class I and II events (black line, with t_{center} = 6 seconds) and class III (gray line with t_{center} = 4 seconds).

respectively, insufficient warning time), 1/2 for $t_{warn} = t_{center}$, and zero for $t_{warn} \gg t_{center}$ (large warning time) (Figure 4). K is either zero if the estimated class is equal to the expected class (i.e., correct classification) or one otherwise; L is a constant of value one for expected class I, II, or III events and zero for expected class 0 events. Finally, S is the spread parameter of the sigmoid function that governs how strongly it spreads over time and W_i is the weight associated with event i. By minimizing the cost function in equation (1), we maximize at the same time both the number of correct classifications and the available warning times. The final cost for the EEW system is thus given by the weighted sum (normalized to unity) of these individual earthquake costs, with weights chosen such that the expected warning classes are equally weighted rather than the individual events.

[27] The cost of each earthquake in the dataset is set to the maximum value of one if it is not correctly classified (K = 1). Warning times are evaluated only for correctly classified events (K = 0). Correct classification is considered as a fundamental precondition before warning times are evaluated because large numbers of false and missed alarms are socioeconomically unacceptable even if the warning times for the remaining correctly classified events are excellent.

[28] For class II and class III events, only the warning times of class II, respectively, class III are considered (and not the warning times of the lower classes that are automatically declared as well) since the warning time that really matters is the one for the final class. The parameter L (L = 0 for class 0 events, L = 1 otherwise) is needed to deal with the events of class 0, where no warning by the system should be declared. If such an event is correctly classified, there is no warning time to be evaluated, and the individual cost for this specific event will be zero because K = 0. If a class 0 event is overestimated and leads to a false alarm, the (nonweighted) individual cost for that event will be one, since K = 1 and L = 0 and the available warning time will not be evaluated since no warning is desired for such an event.

[29] The weighting of events in equation (1) is necessary because the number of class 0 events is much larger than the number of class I, II, or III events. This is also to be expected in reality since small events that should not trigger the system are more abundant than large ones that should do so. If all earthquakes would be equally weighted, the class 0 events would clearly dominate the evaluation scheme. Therefore, we chose to assign equal weights to the four classes of expected ground motion in Istanbul rather than to all events:

$$W_i = \frac{1}{4} \cdot \frac{1}{N_{class(i)}}, \tag{3}$$

where $N_{class(i)}$ is the total number of earthquakes falling into the warning class of event i (N_0 = 79, N_I = 46, N_{II} = 28 and N_{III} = 27 for classes 0, I, II, and III, respectively). The sum of the weights for all events equals one.

[30] Instead of using a sigmoid function in equation (1), the warning times could also be evaluated with a linear function, which might appear more logical at first glance. However, for a given EEW application, the usefulness of the warning time is not necessarily steadily increasing with increasing warning time. For instance, if a warning time of 5 seconds is enough to cut the flow of a gas pipeline, the availability of 15 seconds does not provide an enormous additional gain for this specific application. In such a case, it is preferable to design an EEW system that provides overall somewhat shorter warning times (as long as they are larger than 5 seconds in that case), but is highly robust, rather than a system providing very large warning times for a subset of events, but with lower overall reliability. For this reason, we decided to use a sigmoid function in order to evaluate the warning times. The center time t_{center} of the sigmoid in equation (1) can be chosen based on the application in mind and the spread of the function based on the tolerance of warning times lower than t_{center}.

[31] For the demonstration of our approach on the example of Istanbul, we chose t_{center} based on consideration of the local seismotectonic setting. For each event, we assumed that at every onshore grid point a hypothetical seismic station were available. For a given trigger threshold, we determined the time when this trigger threshold was first exceeded at three hypothetical stations and considered this time as the earliest theoretically possible time when a warning can be declared. This gave us the largest theoretically possible warning times for all events and warning classes in the database.

[32] For trigger thresholds in the range of 0.01–0.15 g, the largest theoretically possible warning times range between 0 and 20 seconds with a median of about 7–8 seconds for all classes (Figures 5a–5c). A further increase of the trigger threshold to, for instance, 0.2 g leads to a decrease of the median to about 5 seconds for class III events (Figure 5d). Since we cannot exclude that the optimal trigger threshold for class III might be located in the upper part of the considered range (0.01–0.32 g) and these largest theoretically possible warning times cannot be reached with a realistic network of a much smaller number of sensors, we decided to use t_{center} = 6 seconds for class I and II warning times and

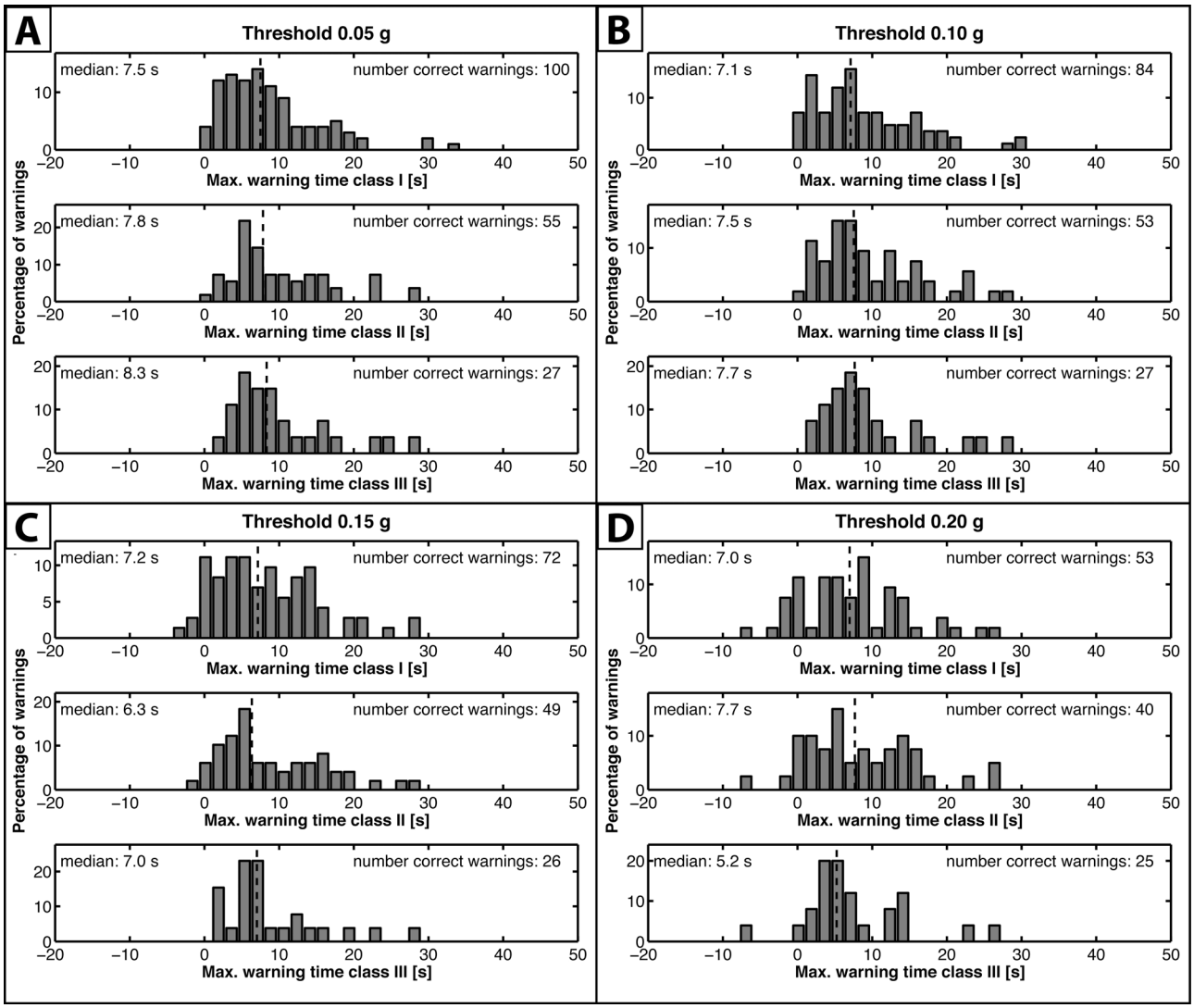

Figure 5. Distribution of the largest theoretically possible warning times considering a hypothetical network with stations at all onshore grid points, thus covering the entire region of interest, for four different trigger thresholds ((a) 0.05 g, (b) 0.10 g, (c) 0.15 g, (d) 0.20 g). For each of these trigger thresholds, these largest theoretically possible warning times have been computed for all three warning classes and the median of each distribution is indicated with a dashed line.

t_{center} = 4 seconds for the evaluation of class III warning times. The spread parameters S of the sigmoid function was set such that the function in equation (2) reached the plateau value of one (maximum nonweighted individual cost) for any warning time lower than 0 seconds. With these definitions, a warning time of class I and II is assigned zero cost if it is larger than about 12 sec (since then there is no cost reduction anymore), and one of class III is regarded as optimal if it is larger than 8 sec. We also investigated the influence of choosing larger t_{center} values (for instance t_{center} = 8 seconds for class I and II and t_{center} = 6 seconds for class III).

5.2. The Microgenetic Algorithm (MGA) Optimization Procedure

[33] For the optimization of sensor locations and trigger thresholds (i.e., finding sensor locations and trigger thresholds providing minimum cost as defined above), we used a microgenetic algorithm (MGA) [*Krishnakumar*, 1989]. MGAs belong to the general class of genetic algorithms (GAs) [*Goldberg*, 1989], which are guided search techniques based on evolutionary principles (survival of the fittest individuals, genetic recombination of these, and mutation) to find models that minimize a given cost function.

[34] Typically, a GA starts with a random population of test models, called chromosomes, which can for instance consist of binary representations of the different model parameters (in that case, each bit is usually termed as a gene). Each chromosome is evaluated and associated with a cost. The fittest chromosomes (i.e., those with lowest cost) are allowed to mate and exchange genetic information via a crossover operator, which leads to a given number of offspring. These offspring are then subjected to a mutation operator and finally form the new generation, and the process restarts (for further details on genetic operators, see, e.g., *Haupt and Haupt* [1998]). Over many generations, the

population will lose diversity and converge to a state of minimum cost, in our case corresponding to optimum sensor locations and trigger thresholds. However, no guarantee can be given that the global minimum will be found, so that a careful analysis of the variability of solutions obtained from several independent runs of the code is indispensable.

[35] As a general rule, the population size of a genetic algorithm should scale exponentially with the number of genes within each chromosome in order to maintain a reasonable degree of genetic diversity over many generations, so that the algorithm does not prematurely converge into a local minimum [*Goldberg*, 1989]. If the number of model parameters and hence the length of the chromosomes increases above a certain level, this may lead to population sizes which are computationally unacceptable since the convergence of very large populations may need a very large number of cost function evaluations and a lot of memory.

[36] A MGA is a variant of a GA which avoids these problems and has been proven to perform equally well or even better than classic GAs for a range of optimization problems [e.g., *Krishnakumar*, 1989; *Carroll*, 1996; *Abu-Lebdeh and Benekohal*, 1999; *Alvarez*, 2002]. An MGA works very similarly to a classic GA, except for the fact that it uses very small population sizes. Such small populations are not able to maintain genetic diversity for very long and generally converge within few generations. When the algorithm has converged, the population is reinitialized to a random state except for the fittest chromosome, which passes unchanged. Hence, the missing genetic diversity is compensated by many restarts of the algorithm. A MGA usually converges with fewer cost function evaluations than a classic GA does.

[37] In our case, the chromosomes consist of the sensor locations for an EEW system with a given number of stations and the set of three trigger thresholds. For the sensor locations, we searched the 128 grid points for potential onshore stations and, if OBS were considered, the 112 offshore grid points within the Sea of Marmara for the location of these sensors. The search range for the three trigger thresholds was 0.01–0.32 g, with intervals of 0.01 g.

[38] We used a MGA with binary encoding, a population size of fifteen chromosomes, uniform crossover with a probability P_{cross} = 0.95 and no mutation. The algorithm was defined to have converged when less than 5% of the genes differed from one chromosome to another within one generation and in that case, the population was reinitialized.

[39] The algorithm was run ten times for each investigated case with different random seed for 5,000 generations. For the first time after 1,000 generations and then every 500, we checked whether the fittest chromosome had improved by more than 1%. If this was not the case, the algorithm was completely reinitialized, including the fittest chromosome. With this procedure, we assess in each case a total of more than 700,000 EEW system configurations and put a strong emphasis in sampling the search space in order to obtain a set of best solutions rather than one single optimum one only. In each case, the 1,000 best solutions were analyzed to assess the stability of the minimum cost EEW system configuration, both in terms of station distribution and trigger thresholds.

[40] We finally note that our current scheme for evaluation and optimization assumes a fully functional EEW system. Failures of individual stations are significantly complicating the situation and a full treatment of this problem would need to take into account random station failures during the simulated scenario earthquakes. One solution to deal with this problem would be calculating, for each station configuration, the cost for the system when a given number of stations (e.g., two) fail, repeat this calculation for the failure of all possible subsets of that number of the network, and use, for instance, the cost of the worst case or the median value as final estimate for the cost of this particular system configuration. However, this procedure would involve a strong increase in computation time, since the evaluation of one EEW system configuration would need several or even many cost function evaluations, increasing severely with increasing number of stations and potential station failures.

6. Results and Discussion

6.1. Performance Evaluation of the Current IEEWS

[41] Using the simulated ground motion time series, we find that the available warning times for the current IEEWS range from 0 to 17 seconds (Figure 6a). On average, ~7.5 seconds warning time are available of events in class III (i.e., most severe ground shaking in Istanbul). However, a serious drawback of the current IEEWS is that it tends to produce a large number of false class III alarms (~2.5 times more class III warnings than expected), and thus strongly overpredicts the ground motion level in Istanbul (Figure 6). In terms of the previously defined classification of severity of shaking in Istanbul, only ~54% of all events are correctly classified by the IEEWS (Figure 7, Table 1). Note that this result depends on the previously discussed choice of class definition thresholds for the ground motions in Istanbul assigning each event to class 0, I, II, or III (i.e., on the choice of what level of ground motion is considered as severe). Thus the current IEEWS is highly sensitive to small and moderate ground shaking, declaring alarms of the highest category also for many events with PGA in Istanbul well below 0.1g.

6.2. Evaluation and Optimization of Trigger Thresholds

[42] From a systematic search over different trigger threshold combinations while keeping the sensor locations of the current IEEWS fixed, we find that the performance is best if the trigger thresholds are set to 0.03, 0.12, and 0.16 g (compared with 0.02, 0.05, and 0.1 g of the current IEEWS). We searched the trigger threshold range 0.01–0.32 g with increments of 0.01 g and under the constraint that the class II and III thresholds are larger than the class I and II ones, respectively. These new thresholds lead to an overall cost reduction of ~23% as compared with the current IEEWS (Figure 7, Table 1). Though the warning times are somewhat decreased due to the higher trigger thresholds for classes II and III (Figure 8), more than 80% of all events are now correctly classified (Figure 7). This outcome clearly shows that, for a given EEW system with given seismic network layout, the appropriate choice of the system parameters

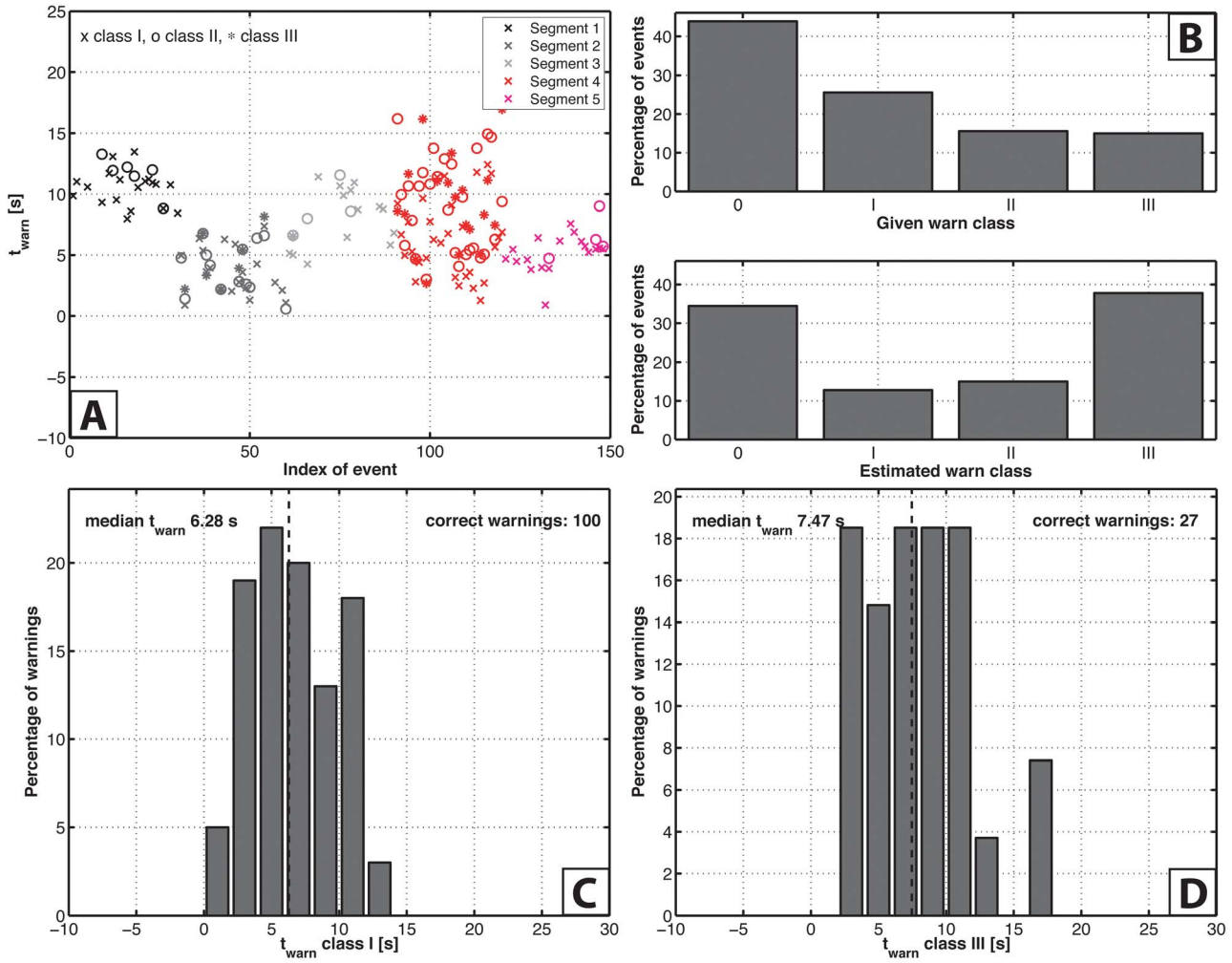

Figure 6. Performance of the current IEEWS on the simulated dataset. (a) Warning times for the 150 earthquakes bound to the five segments of the North Anatolian fault beneath the Sea of Marmara. (b) Comparison of the percentage of expected events in each warning class (top) and the estimated percentage by the EEW system (bottom). (c) Distribution of the warning times for class I warnings; the median is indicated with a dashed line. (d) Same as (c) for class III warnings.

governing the warning declarations plays a crucial role in the performance of the system.

6.3. Evaluation and Optimization of the Seismic Network

[43] We use the MGA to study several scenarios, including the supplementation of the current IEEWS with six onshore or three ocean bottom seismometers (OBS) in the Sea of Marmara (Figure 7, red), or designing completely new EEW systems with five to fifteen sensors, respectively (Figure 7, blue). We also investigate a network with seven onshore and three OBS stations (Figure 7, magenta).

6.3.1. Different Numbers of Onshore Sensors

[44] We find that at least six onshore sensors are required for obtaining a performance level approaching the one of the current IEEWS with optimally chosen trigger thresholds (Figure 7, Table 1). For eight or more stations, the same group of seven to eight sites always dominates in the 1,000 best EEW system configurations, and this group does not significantly change when further increasing the number of sensors. In particular, the optimum network configuration found for a system with ten stations shows striking similarities with the current IEEWS (Figure 3a), but its classification performance is strongly improved: while the current IEEWS overestimates most class I and II events to be class III (Figure 3b), this effect disappears in the optimized system, mainly because of higher trigger thresholds (0.03, 0.12, and 0.2 g compared to the current thresholds of 0.02, 0.05, and 0.1 g) (Figure 3c). However, as a consequence of higher trigger thresholds the warning times for the class III events are reduced by ~2.0–2.5 seconds on average (Figure 9).

[45] The performance of the considered EEW systems with eight or more sensors does not significantly increase with increasing number of sensors (Figure 7). Indeed, a comparison of the available warning times for the optimal sensor configuration found for fifteen stations with the one for ten stations (Figure 10) indicates that, while on average the warning times of class I and II show a slight improvement when increasing the number of sensors, the opposite is true for class III events.

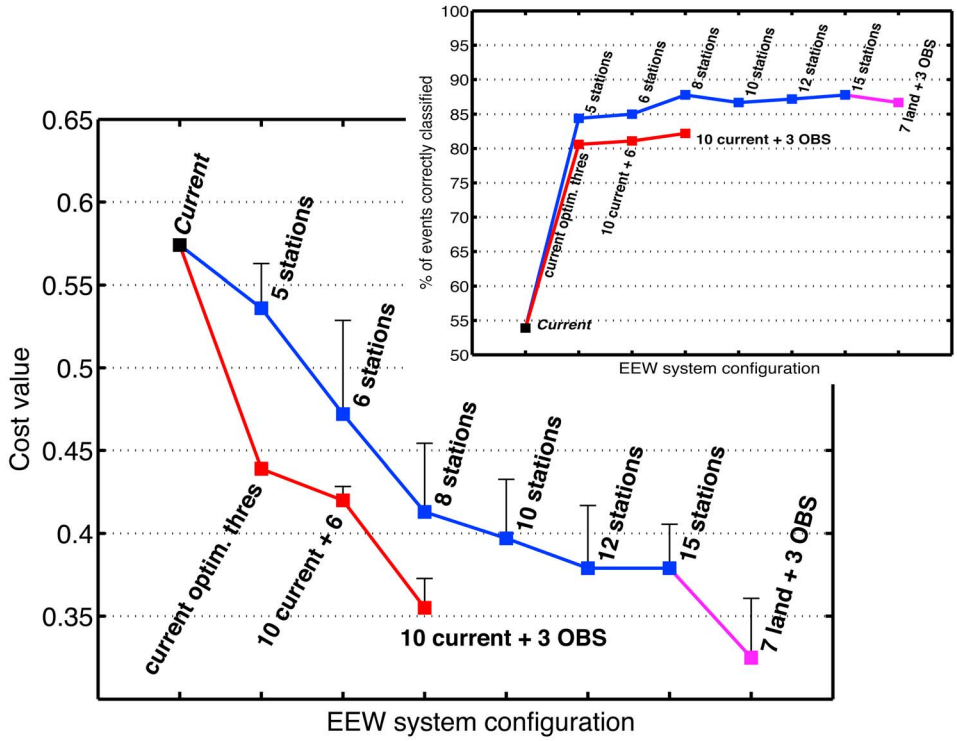

Figure 7. Costs (i.e., quantitative measure of performance) of the best EEW system configurations found by the optimization approach. Black square: cost of the current IEEWS. Blue squares: costs of the best EEW system configuration for fully optimized systems with different numbers of stations (best solution found in ten MGA runs, trigger thresholds are also optimized). Magenta square: cost of best configuration for a system of seven onshore stations and three OBS. Red squares: costs of EEW system configurations including the current ten sensors. For each case, the thin black line indicates the cost range of the 1,000 best solutions found in the MGA runs (except for the current system with optimized thresholds, since in that case no MGA optimization, but a systematic search over a fixed number of trigger threshold combinations, was performed). Inset: Percentage of correctly classified scenario events for the different lowest cost EEW system configurations.

[46] When more sensors are available, each fault segment can be more densely instrumented, whereby moderate events further away from Istanbul, causing only moderate ground motions in the city for which class I or II warnings are expected, can be detected more timely. However, such events can cause large ground motions close to the source, and setting up a denser network therefore leads to the necessity of increasing the class III trigger threshold (as

Table 1. Results from the Evaluation and Optimization of EEW Systems with Different Numbers of Onshore Sensors and Under Consideration of OBS[a]

Configuration	$Cost_{min}$	Cost range 1,000 best models (in % of $Cost_{min}$)	A_1 (g)	A_2 (g)	A_3 (g)	$fact_{OBS}$	% Events correctly classified
Current	0.574	/	0.02	0.05	0.10	/	53.9
Current optimal thresholds	0.439	/	0.03	0.12	0.16	/	80.6
5 onshore stations	0.536	5	0.03	0.07	0.19	/	84.4
6 onshore stations	0.472	12	0.02	0.10	0.17	/	85.0
8 onshore stations	0.413	10	0.03	0.10	0.17	/	87.8
10 onshore stations	0.397	9	0.03	0.12	0.20	/	86.7
12 onshore stations	0.379	10	0.04	0.12	0.21	/	87.2
15 onshore stations	0.379	7	0.04	0.13	0.24	/	87.8
10 existing stations + 6 onshore stations	0.420	2	0.04	0.12	0.17	/	81.1
10 existing stations + 3 OBS	0.355	5	0.03	0.12	0.26	1.0	82.2
7 onshore stations + 3 OBS	0.325	11	0.03	0.08	0.20	1.4	86.7
10 onshore stations with t_{center} = [8 8 6] s	0.530	5	0.04	0.16	0.31	/	75.0
7 onshore stations + 3 OBS with t_{center} = [8 8 6] s	0.458	8	0.03	0.13	0.20	1.3	83.3

[a]Shown is the minimum cost in case of optimization runs the cost range of the 1,000 best solutions and the three trigger thresholds of the optimal system configuration (A_1, A_2, A_3). When also considering OBS, the scaling factor $fact_{OBS}$ between trigger thresholds onshore and for OBS is also shown.

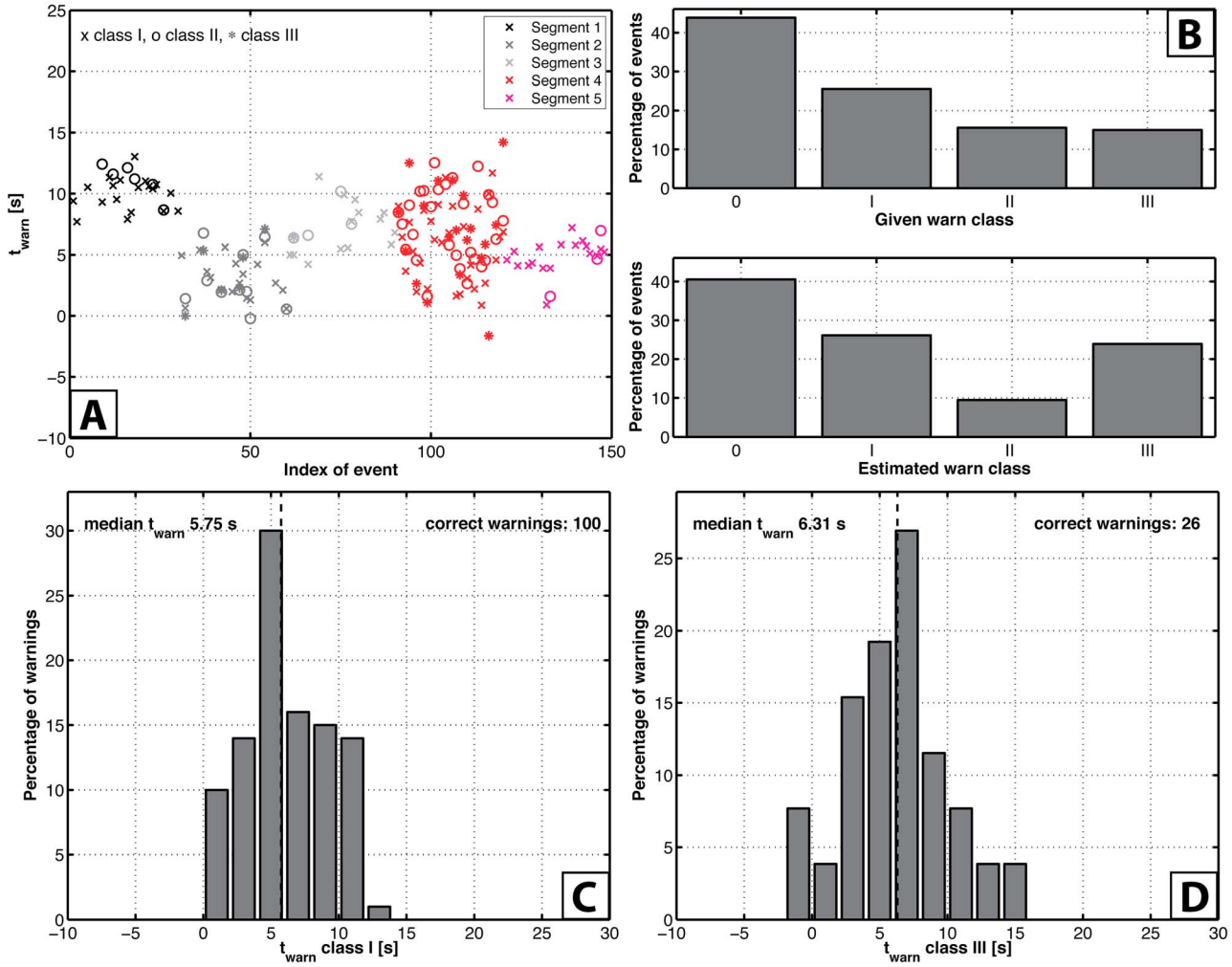

Figure 8. Same as Figure 6, performance of the IEEWS with optimized thresholds.

observed in the optimization runs with increasing number of stations, Table 1) in order to avoid false alarms for Istanbul, as there may be three or more sensors located near the epicenter. In return, an increase of the class III trigger threshold leads to the observed decrease of the average available warning time for class III events.

[47] No matter what the tested number of sensors is, the overall classification performance is always better than 80% if the trigger thresholds are appropriately chosen, even though generally slightly more events are correctly classified when designing a completely new system rather than involving the sensor locations of the current IEEWS (Figure 7).

6.3.2. Variability Analysis of the Solutions

[48] For each investigated EEW system variant, we obtain from the MGA runs an optimal system configuration with lowest cost. This optimal solution, however, may not be the only good solution, as it is a common situation that the cost function shows several distinct (or even numerous) local minima. For this reason, we performed ten independent runs of the MGA as described above and investigated the variability of the 1,000 best solutions.

[49] For this purpose, we determined the relative frequency of each potential station location on the grid in the 1,000 best EEW system configurations. For different numbers of sensors, we generally found a consistent pattern in the grid points dominantly contributing to the 1,000 best solutions (Figure 11), and this pattern also clearly appears in the corresponding minimum cost solution (Figure 12). For only five sensors, there is basically no choice where to deploy them, and the variability in the 1,000 best solutions is very small. For six sensors, there is considerably more variability, which, however, decreases again when moving on to a system of eight sensors. From eight to fifteen sensors, there is a consistent pattern of about eight sites that dominate in the set of 1,000 best solutions: a cluster of three stations southwest of Istanbul, another cluster on or around the Prince's Islands southeast of Istanbul, and one to two sites on the Yalova peninsula (opposite to Istanbul, Figure 1) (Figure 11). This clustering into groups of at least three stations is not very surprising, since our EEW algorithm requires three sensors to exceed the trigger threshold within 5 seconds before declaring an alarm. Therefore, sets of three stations have to be close enough to each other to

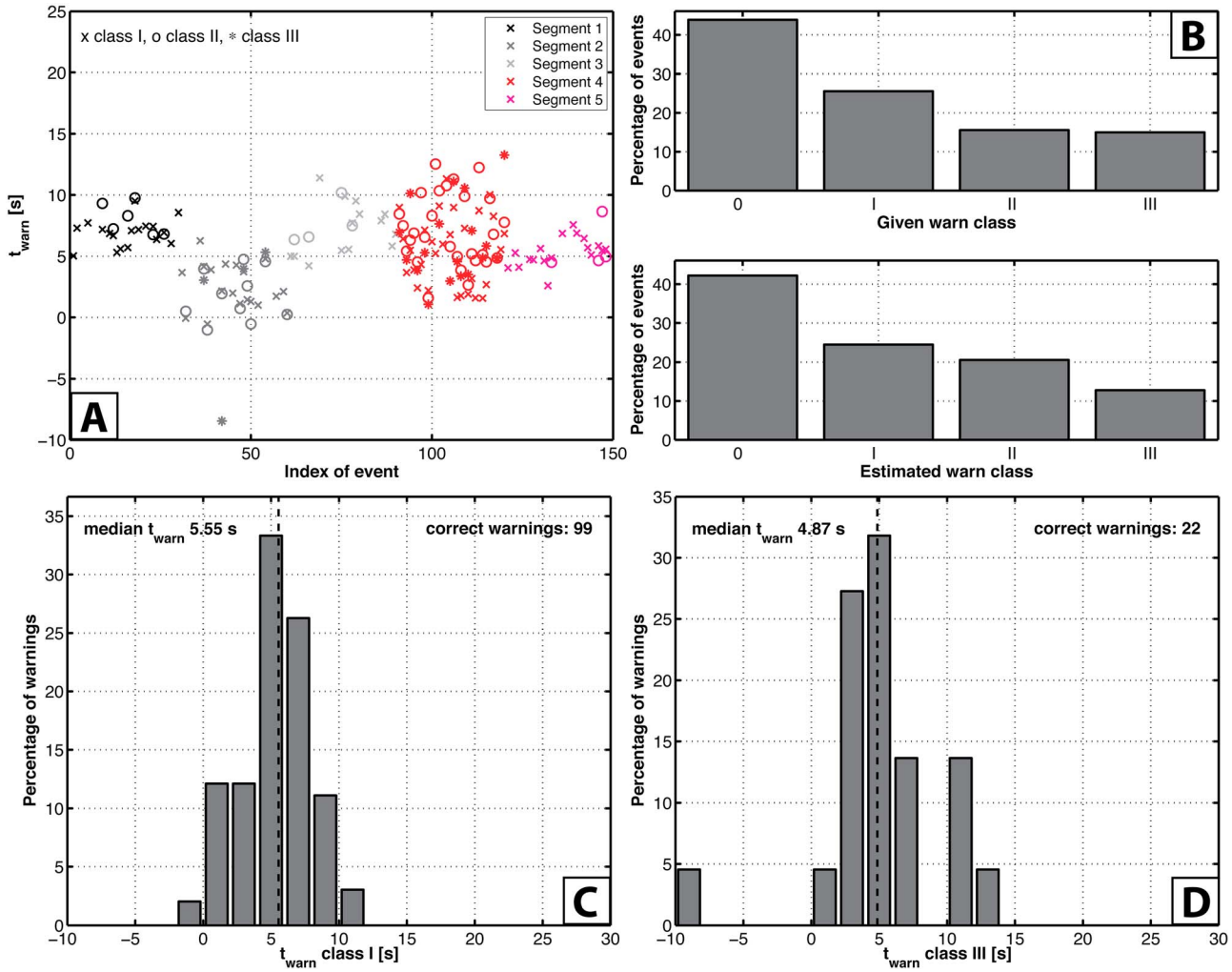

Figure 9. Same as Figure 6, performance of the optimized EEW system consisting of ten stations.

satisfy this condition. This result and the fact that there is no significant decrease in the cost for a number of sensors exceeding eight to ten stations (Figure 7, Table 1) suggests that no significant performance improvement can be expected using this EEW algorithm with a larger number of sensors.

[50] The stability analysis of the trigger thresholds found in the 1,000 best solutions (Figure 13) shows strong similarities with the stability analysis of the sensor locations (Figure 11): the variability increases when increasing the number of sensors from five to six, but decreases again when considering eight or ten sensors. In general, the trigger threshold for class I is the most stable, indicating that the discrimination between class 0 (no warning) and class I events works very well.

6.3.3. Supplementing the Current Seismic Network

[51] We find that supplementing the current IEEWS network for instance with six additional sensors hardly achieves any enhancements compared to the current system with optimized trigger thresholds. When considering the case of supplementing the current IEEWS network with six sensors, four of these are consistently placed on the Yalova peninsula (Figure 14a), and the 1,000 best configurations show very little variability both in station distribution (Figure 14b) and trigger thresholds (Figure 14c). However, compared to the current IEEWS with optimized trigger thresholds, there is only a negligible performance increase (less than 5% of reduction in cost, Figure 7), and the trigger thresholds are practically identical (Table 1). This result clearly suggests that no significant performance increase can be expected when supplementing the existing network of ten sensors with additional stations.

6.3.4. The Usage of Three Ocean Bottom Seismometers

[52] We tested two supposed cases: first, we considered adding three OBS to the current IEEWS network and searched for their optimal positions within the Sea of Marmara and the optimal trigger thresholds. Second, we optimized a completely new system consisting of seven onshore stations and three OBS.

[53] When considering the usage of OBS, we introduced a further variable into the optimization, namely a scaling factor between the trigger thresholds for onshore stations and the OBS, $fact_{OBS}$, since the OBS will be located much closer to the fault and therefore, higher trigger thresholds have to be expected for these stations. We allowed this

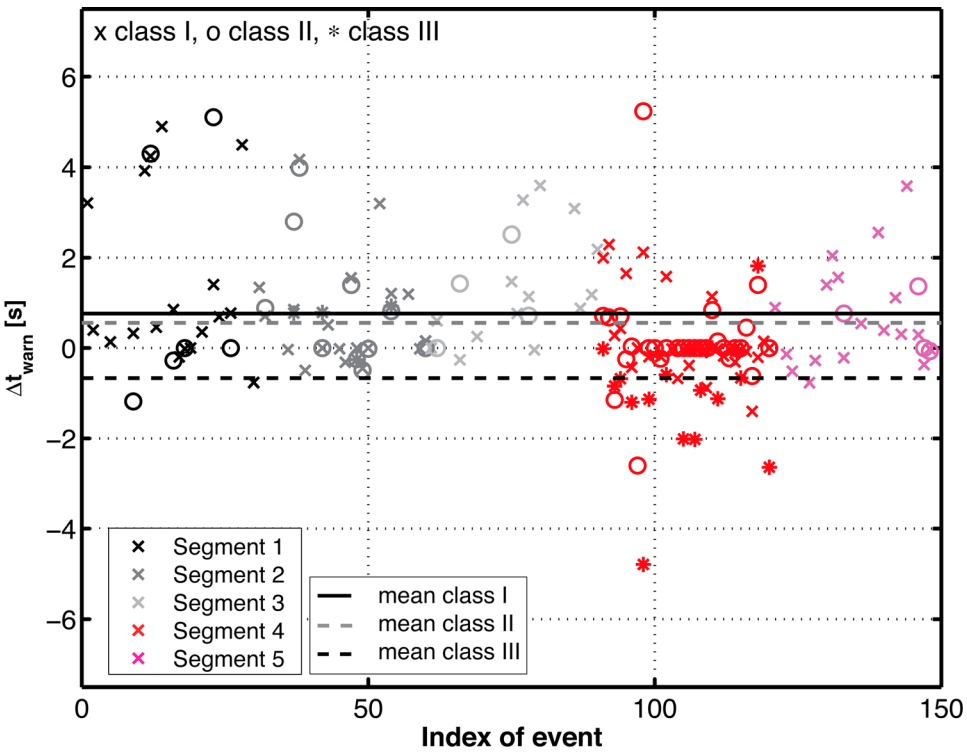

Figure 10. Comparison of the performance in terms of warning times between the best system configuration found with fifteen sensors and the best with ten sensors. Shown is the difference in warning time, $\Delta t_{warn} = t_{warn,15} - t_{warn,10}$, for each correctly classified event (given by the index of the event from 1 to 150, with 30 events on each of the five segments. The three lines (see legend) show the mean Δt_{warn} for the three different classes. These indicate that the mean warning times for class I and II are slightly better for the system of fifteen sensors, while the mean warning times for class III are better for a system of ten sensors.

factor to range between one (equal trigger thresholds) and two (double trigger thresholds for OBS).

[54] Supplementing the current system with three OBS leads to a considerable decrease in cost of close to 20% as compared with only optimizing the trigger thresholds of the system (Table 1). The variability in the locations and trigger thresholds is again very small (Figures 15b and 15c), and the scaling factor $fact_{OBS}$ ranges between 1 and 1.5 (Figure 15c). The median of the warning times shows an increase of about 1.3 seconds as compared with the current IEEWS network configuration and optimal thresholds.

[55] The lowest cost of all considered cases is obtained when optimizing a system of seven onshore sensors and three OBS (Figure 16, Table 1). Almost 87% of all events can be correctly classified with such a system, only some events of class I have been overestimated to be class II (Figure 16d). Again, the obtained station distributions and trigger thresholds for the 1,000 best models are rather stable, even though there is slightly more variability than for a system consisting of onshore stations only (Figures 16b and 16c). The median warning time for class III earthquakes ranges around 7.3 seconds. Compared with the optimum ten sensor system with only onshore stations, the warning time for class III events increases thus by ~2.4 seconds on average.

[56] However, the practical problems in using OBS are considerable (e.g., costs for data transmission or the fact that steep slopes in the bathymetry in some areas of the Sea of Marmara may prohibit the successful deployment of an OBS) which were not considered in our studies. Moreover, other factors such as the appropriateness of the average site response function are difficult to assess in the case of OBS and the ones used for the simulation of the ground motion time histories beneath the Sea of Marmara (NEHRP C) might be problematic as well. Nevertheless, while keeping these drawbacks in mind, our results suggest that the usage of OBS in the Istanbul case might be promising.

6.3.5. The Effect of Claiming Larger Warning Times

[57] All results discussed so far were obtained using t_{center} = 6 seconds for class I and II events and t_{center} = 4 seconds for class III events in the cost function defined in equation (1), which were chosen based on theoretical considerations for a hypothetical network having stations at all grid points.

[58] In order to test the effect of claiming larger warning times, we ran the optimization procedure for an EEW system of ten onshore stations as well as for one of seven onshore and three OBS stations using t_{center} = 8 seconds for class I and II and t_{center} = 6 seconds for class III, thus claiming 2 seconds more of warning time for an event to be associated with the same cost as before.

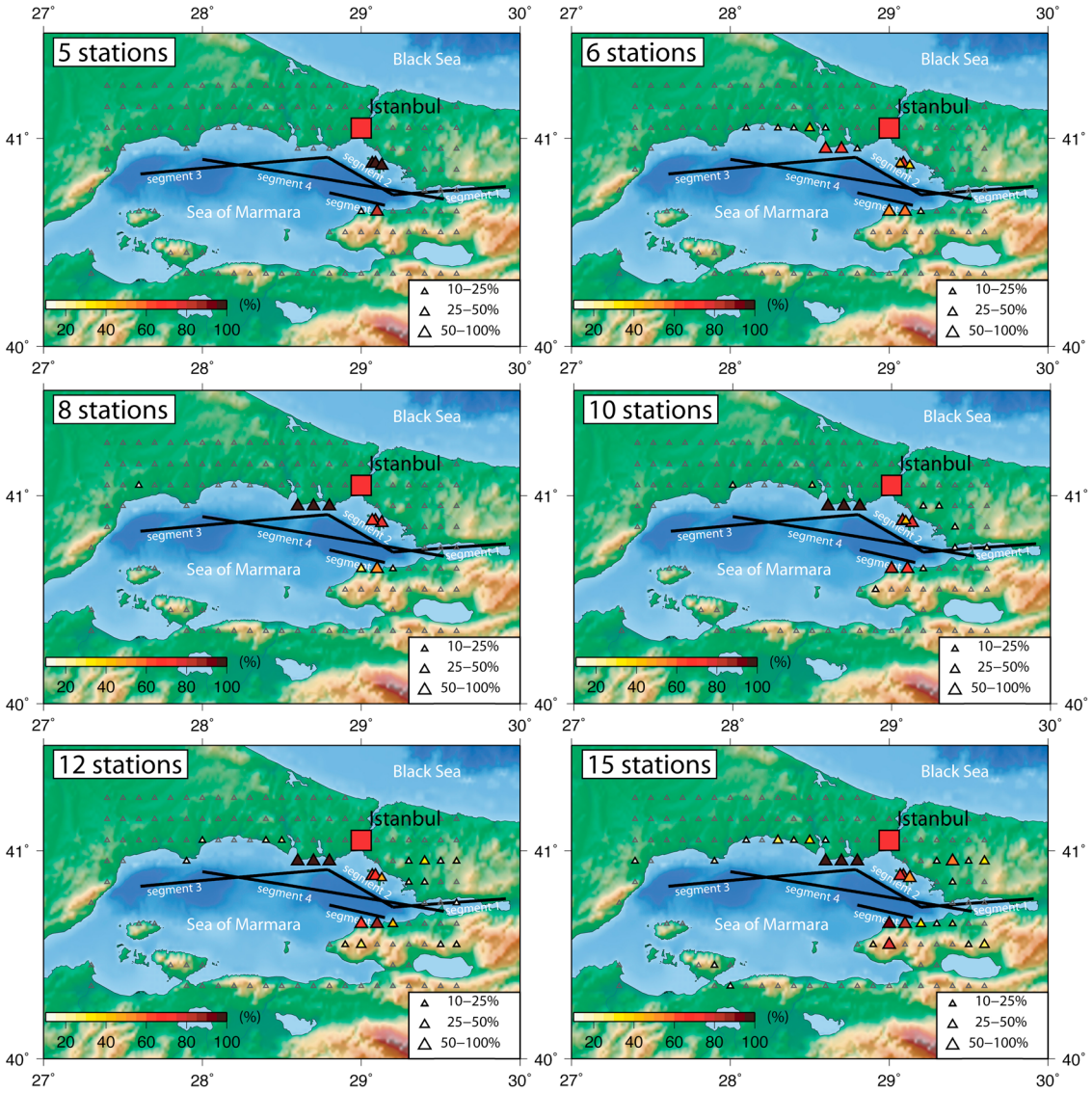

Figure 11. Analysis and comparison of variability in terms of station configuration in the 1,000 best EEW system configurations found in ten independent runs of the MGA for different numbers of stations. Each grid point appearing in more than 10% of the 1,000 best configurations is depicted with a colored triangle, the color and the size of the latter indicating its relevance in the 1,000 best solutions.

[59] The results reveal a strongly modified sensor configuration in the case of ten onshore stations (Figure 17a), with the general effect that the sensors move further away from the user site, downtown Istanbul. Moreover, the Prince's Islands southeast of Istanbul do not show any importance anymore in the results, as can be seen from the optimum sensor configuration (Figure 17a) and the variability analysis for the station configuration in the 1,000 best solutions (Figure 17b). The station distribution as well as the trigger thresholds show stable characteristics (Figures 17b and 17c), the latter being larger for class II and III than previously. However, the most interesting aspect is the fact that the class III events are almost all incorrectly classified (Figure 17d), and that the warning times for the few correct class III events are extraordinarily poor (Figure 17f). This observation can be explained by the fact that most of the class III earthquakes originate on segment 2 very close to Istanbul or on segment 4, which is intended to simulate joint ruptures of segments 1, 2, and 3. These segments are so close to Istanbul that it is impossible to fulfill the requirement of obtaining these longer warning times while keeping the class III trigger threshold at a high enough level so that it does not cause a significant number of class III false alarms. The cost function in equation (1) associates an insufficient warning time with the same cost as a missed alarm (which is effectively the case if the warning comes too late) and the optimization procedure simply ignores these segments, as there is no chance to obtain acceptable warning times following the above definition. Instead, sensors are moved to areas where there is a chance to fulfill the requirements on warning time, which are further away from the city of Istanbul.

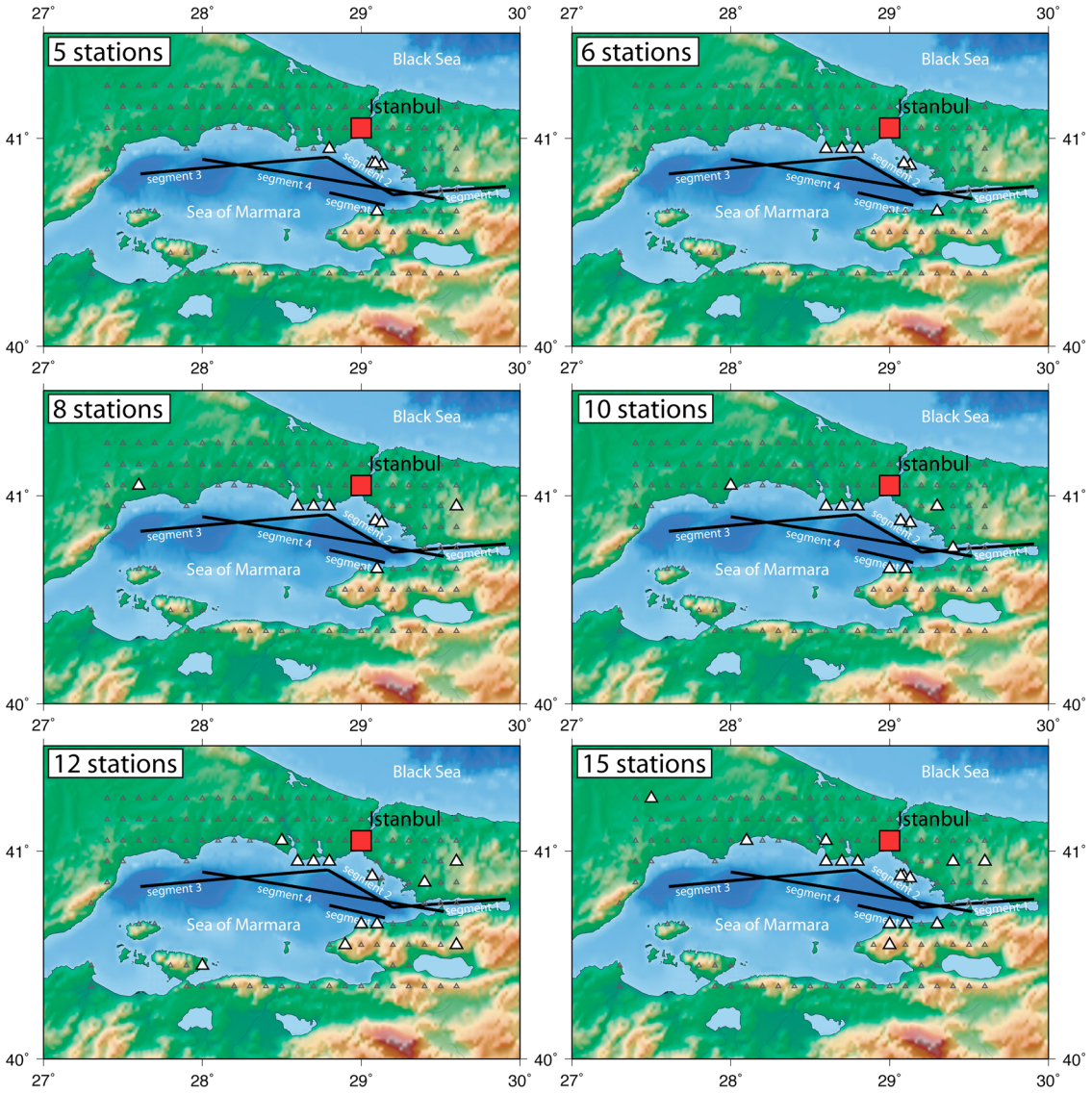

Figure 12. Comparison of the station configuration of the best EEW system found in ten independent runs of the MGA for different numbers of stations.

[60] In contrast, the results for the case of seven onshore and three OBS sensors (Figure 18) look quite similar to the ones for the same system with smaller t_{center} values (Figure 16), however, with lower influence of the Prince's Islands than before, which is again due to the proximity of these to the city of Istanbul. The trigger thresholds are quite similar too (Table 1). The main difference is that the warning times, especially for class II, show a slight improvement (Figures 18e and 18f), however, at the price of a slight decrease in the overall classification performance (Table 1, Figure 18d). In this case, the optimization with the larger t_{center} values still provides reasonable results because, as discussed earlier, the usage of three OBS has the potential to increase the warning times on average by 2 seconds as compared with a system of only onshore stations.

[61] This example shows that there is indeed a trade-off between warning time and system robustness: if, for a given seismotectonic setting, the requested warning times are too large, then the faults for which this problem applies are simply ignored.

7. Conclusions

[62] Our results suggest that the current network layout of the IEEWS is not far from optimal. Furthermore, the current IEEWS is highly sensitive to rather small ground motion amplitudes, declaring warnings of the highest category for events with PGA in Istanbul well below 0.1 g. Therefore, an appropriate increase of the class II and III trigger thresholds together with a potential slight rearrangement of the existing network are likely to have a much stronger impact on increasing the system performance than adding supplementary sensors. Our results also indicate that the usage of three OBS in the Sea of Marmara could improve the system performance (Figure 7) and might increase the available warning times by 2 to 3 seconds.

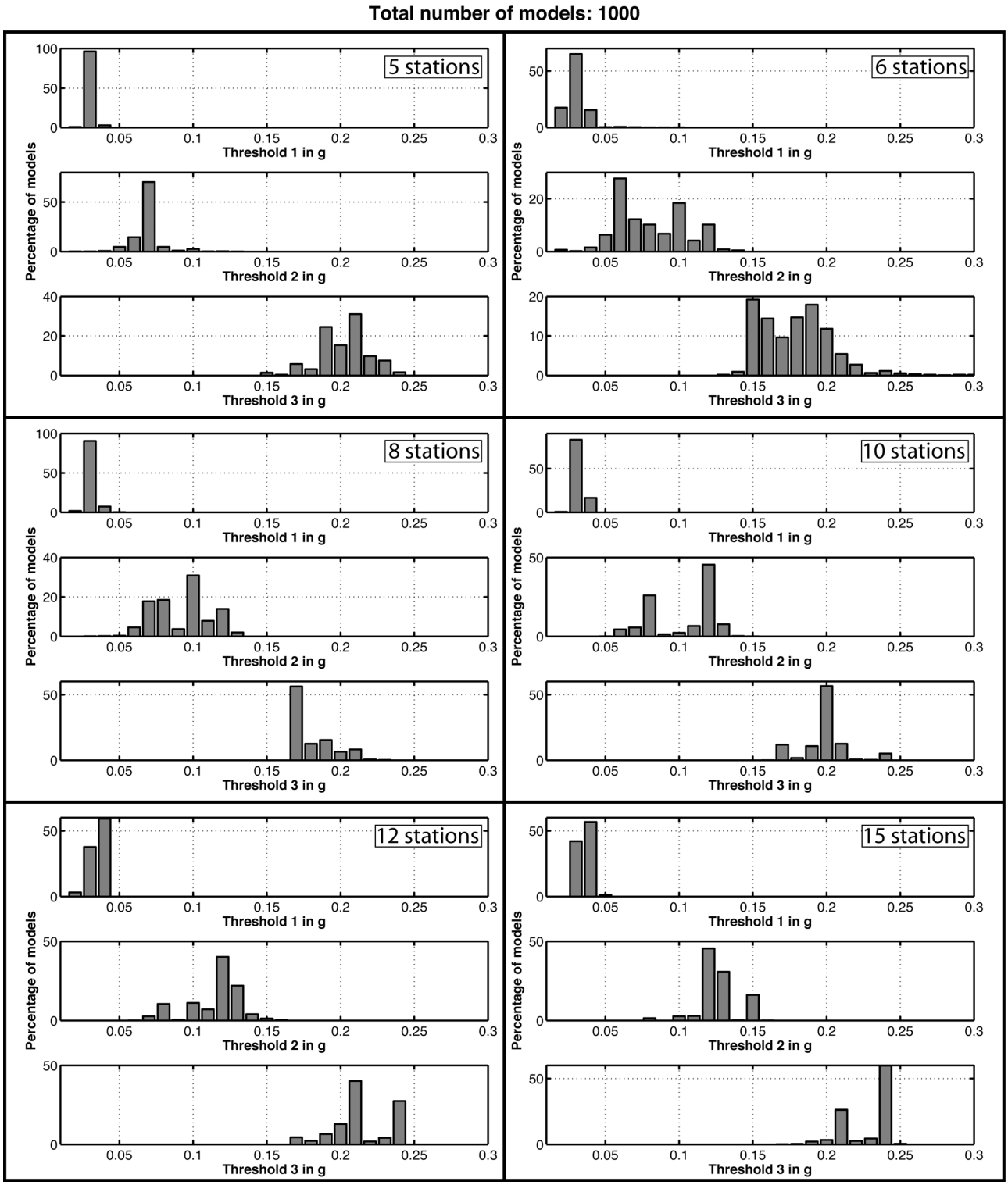

Figure 13. Analysis and comparison of variability in terms of trigger thresholds in the 1,000 best EEW system configurations found in ten independent runs of the MGA for different numbers of stations. Shown are histograms in percent indicating the relevance of each threshold.

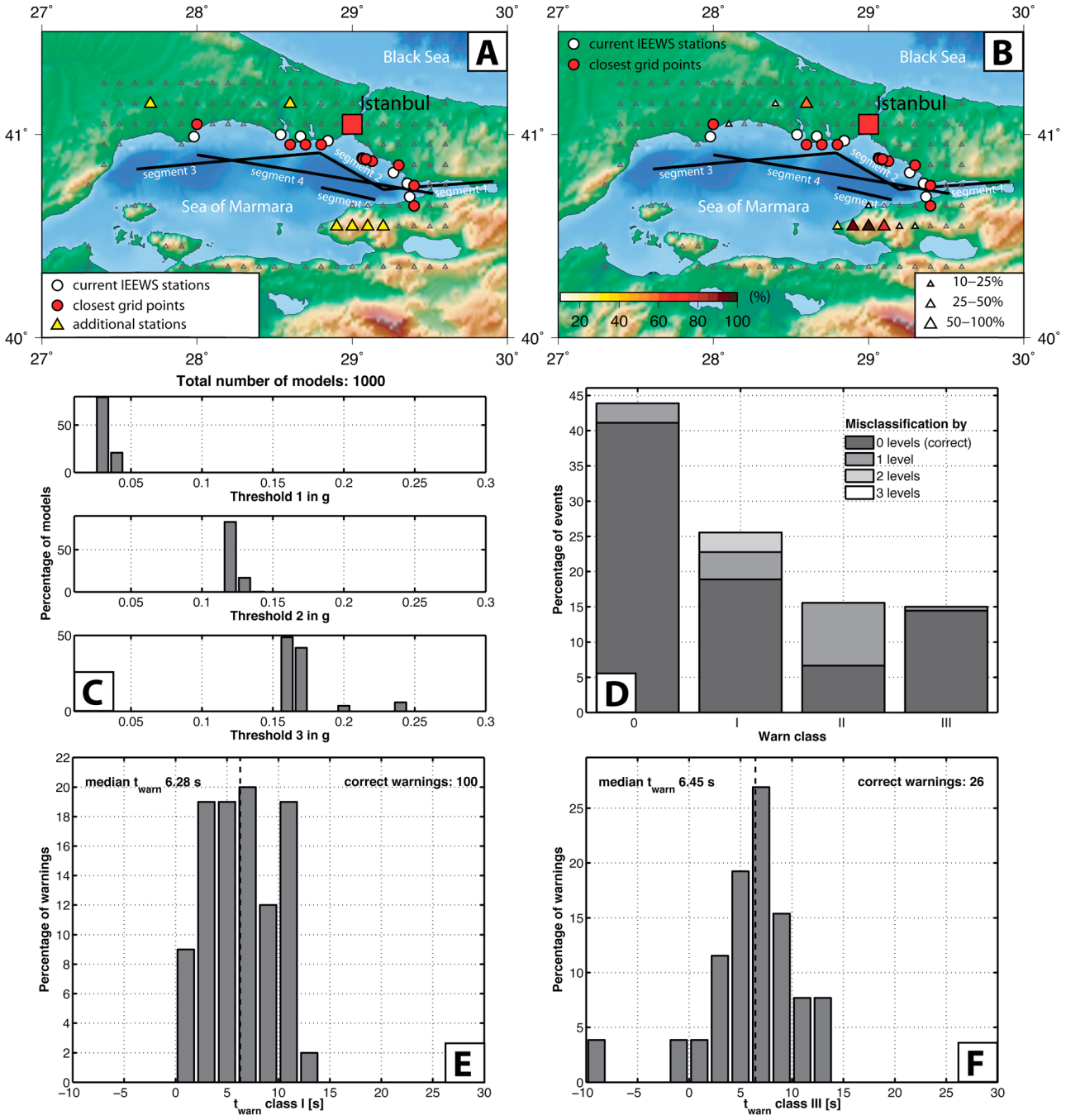

Figure 14. Results of optimization and performance when adding six stations to the current IEEWS sensor configuration and looking for optimal trigger thresholds. (a) Best station distribution found. (b) Variability in sensor configuration in 1,000 best configurations. (c) Variability in trigger thresholds in 1,000 best configurations. (d) Classification errors produced by the best system (see also Figures 3b and 3c for explanation). (d) Distribution of the warning times for class I warnings; the median is indicated with a dashed line. (f) Same as (e) for class III warnings.

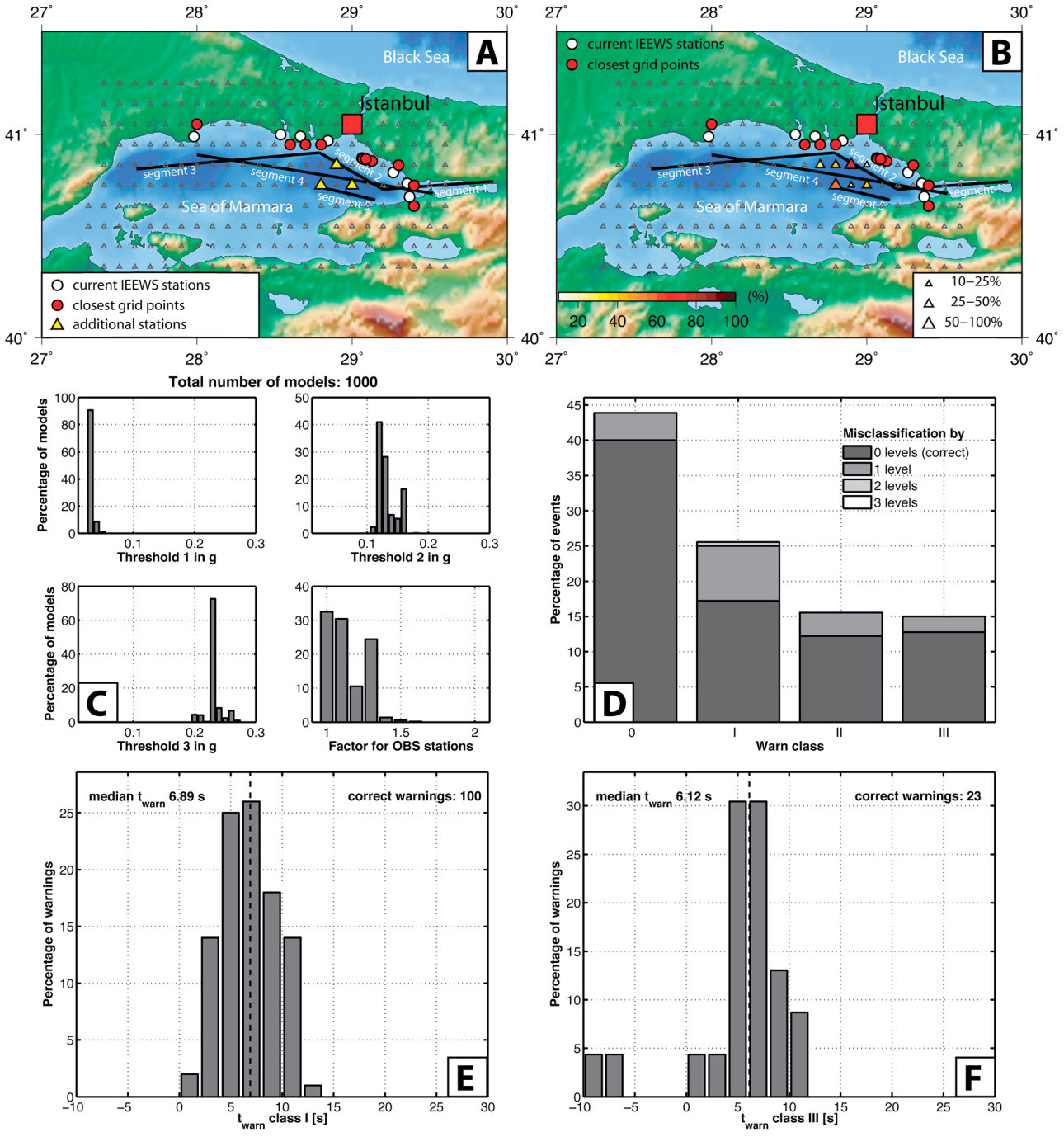

Figure 15. Same as Figure 14, results of optimization and performance when adding three OBS to the current IEEWS and looking for optimal trigger thresholds.

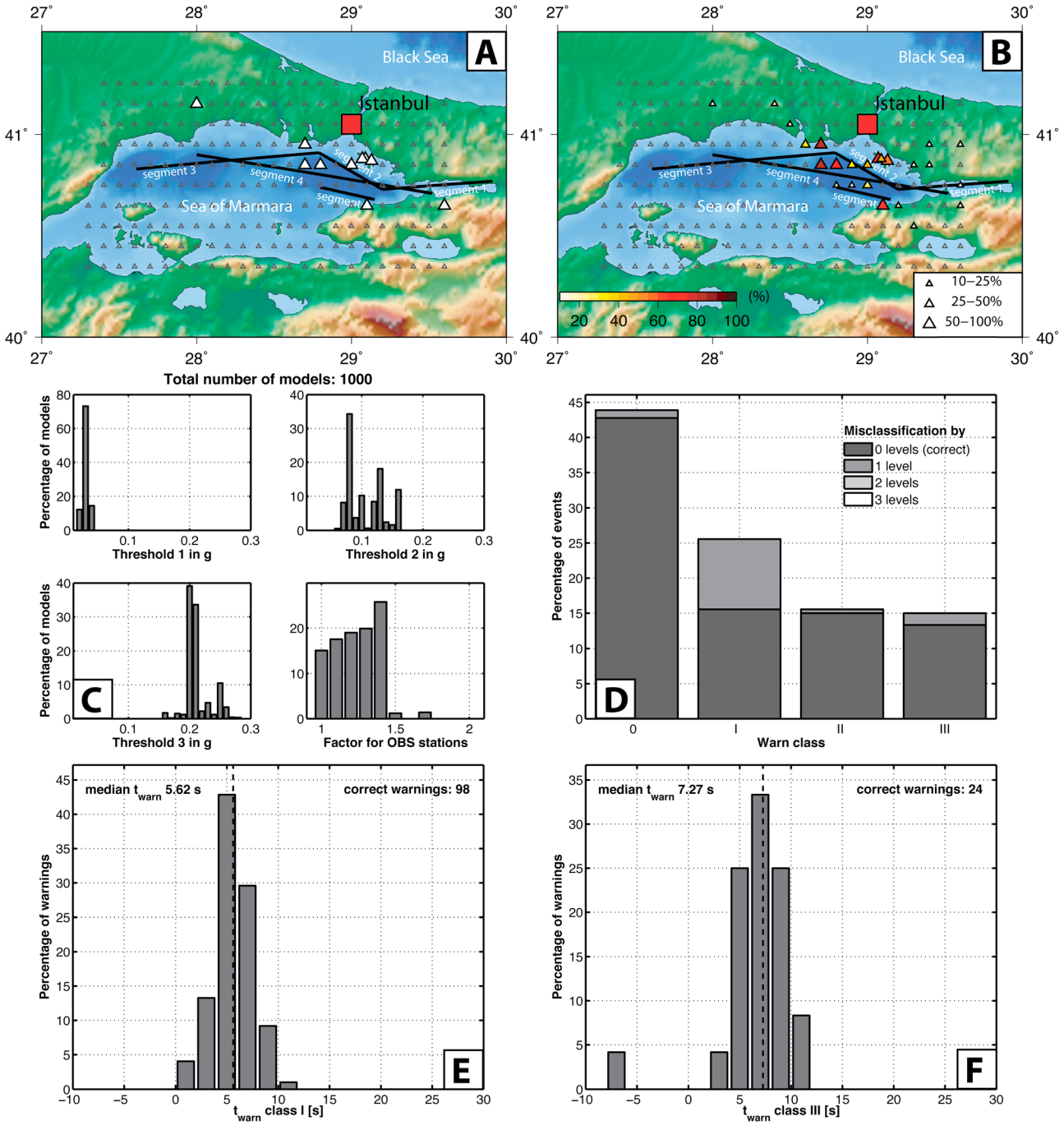

Figure 16. Same as Figure 14, results of optimization and performance of the EEW system when optimizing a system of seven onshore stations and three OBS.

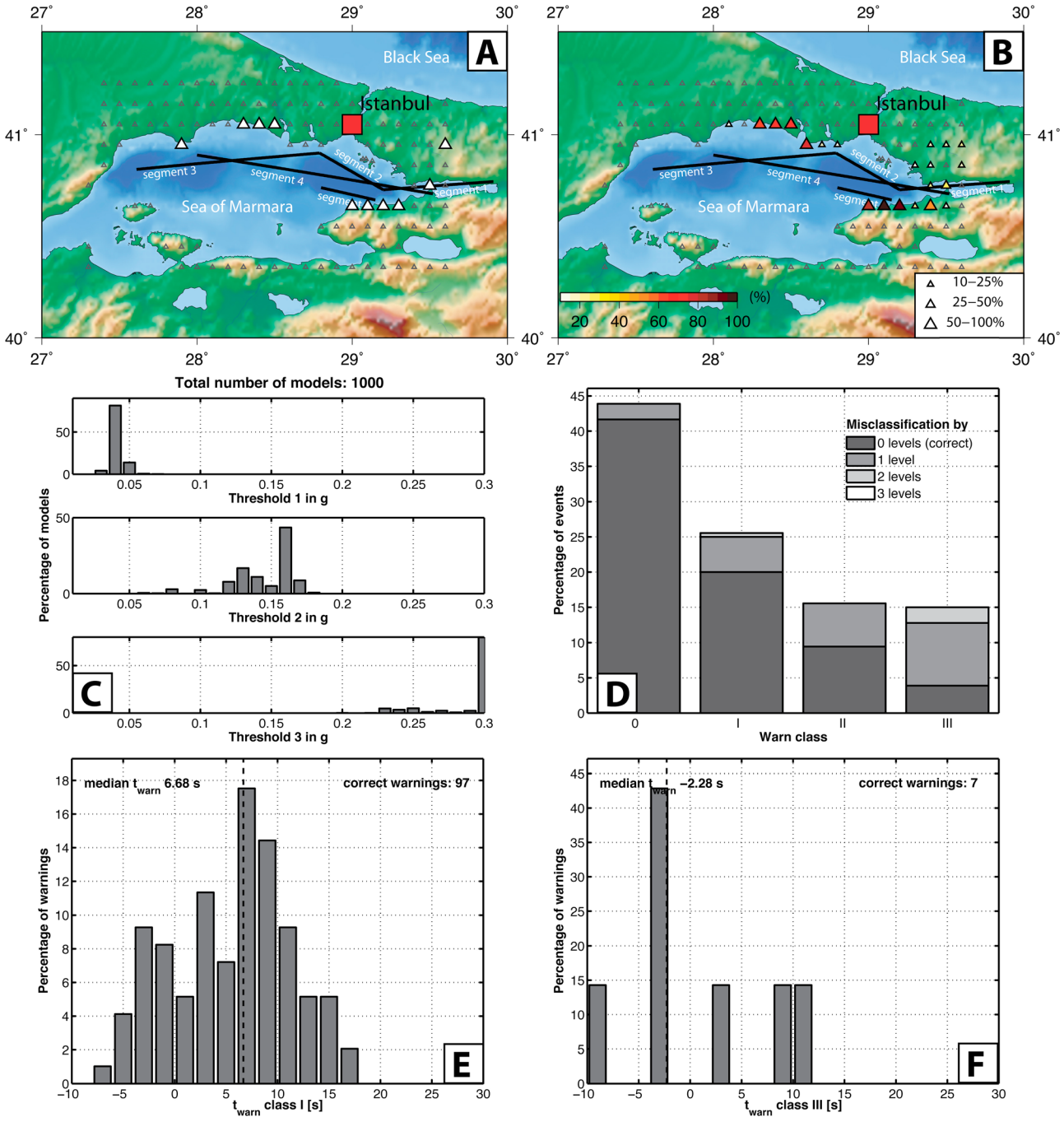

Figure 17. Same as Figure 14, results of optimization and performance of the EEW system when optimizing a system of ten onshore stations with t_{center} = 8 seconds for class I and II and t_{center} = 6 seconds for class III in the cost function.

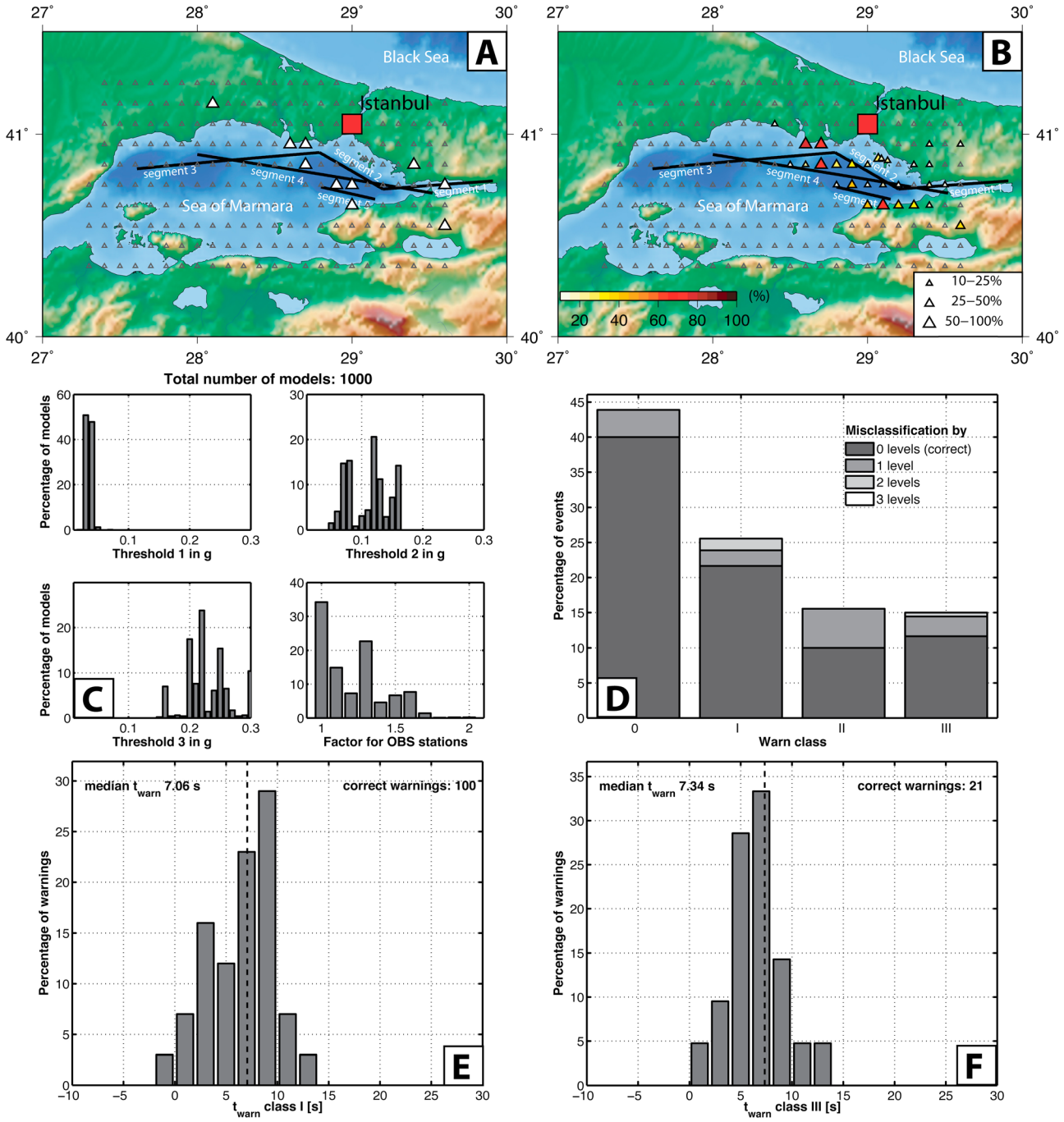

Figure 18. Same as Figure 14, results of optimization and performance of the EEW system when optimizing a system of seven onshore stations and three OBS with t_{center} = 8 seconds for class I and II and t_{center} = 6 seconds for class III in the cost function.

[63] The proposed methodology enabled us to systematically look into the performance and optimization potential of the IEEWS. The technique can also be applied to other EEW systems by adapting the cost function to the respective EEW algorithm and the output it provides. The optimization can also be performed with specific applications in mind. For instance, if a certain automated application, such as cutting pipeline flow, needs a minimum time to be executed, the cost function can be designed to find the optimal system configuration fulfilling these constraints. Moreover, the classification scheme for ground shaking severity does not necessarily have to be based on PGA, as PGA alone is certainly not the best proxy for expected damage potential.

[64] However, a clear requirement of our approach is that the database of synthetic seismograms is appropriate for the corresponding EEW algorithm. For instance, with stochastically simulated time histories as used in this study, a performance evaluation of an EEW system based on magnitude estimation from the predominant period of the early *P*-wave signals [e.g., *Nakamura*, 1988; *Allen and Kanamori*, 2003]

does not make sense, but would require synthetic waveforms with deterministic signals at low frequencies [*Olson and Allen*, 2005]. In such a case, more physics-based ground motion simulations are required.

[65] **Acknowledgments.** The work presented in this article has been carried out within the framework of the EU FP6 project SAFER (Seimic eArly warning For EuRope). The authors wish to thank Stefano Parolai and Dino Bindi for valuable comments that helped to improve an earlier version of this manuscript. Matteo Picozzi checked the seismic noise level on the Ataköy array data in Istanbul for us. Thanks are also due to the associate editor and two anonymous reviewers for constructive comments and suggestions. This publication was supported by the National Research Fund, Luxembourg (FNR/10/AM4/22).

References

Abu-Lebdeh, G., and R. F. Benekohal (1999), Convergence variability and population sizing in micro-genetic algorithms, *Comput. -Aided Civ. and Infrastruct. Eng.*, *14*, 321–334.

Allen, R. M., and H. Kanamori (2003), The potential for earthquake early warning in southern California, *Science*, *300*, 786–789.

Allen, R. M., H. Brown, M. Hellweg, O. Khainovski, P. Lombard, and D. Neuhauser (2009a), Real-time earthquake detection and hazard assessment by ElarmS across California, *Geophys. Res. Lett.*, *36*, L00B08, doi:10.1029/2008GL036766.

Allen, R. M., P. Gasparini, O. Kamigaichi, and M. Böse (2009b), The status of earthquake early warning around the world: an introductory overview, *Seismol. Res. Lett.*, *80*, 682–693.

Alvarez, G. (2002), Can we make genetic algorithms work in high-dimensionality problems?, *Stanford Explor. Proj. SEP Rep. 112*.

Anderson, J. (2003), Strong motion seismology, in *International Handbook of Earthquake Engineering and Seismology*, edited by W. H. K. Lee, H. Kanamori, P. C. Jennings, and C. Kisslinger, Part B, Chap. 57, pp. 937–966, Academic, San Diego, California.

Armijo, R., B. Meyer, S. Navarro, G. King, and A. Barka (2002), Asymmetric slip partitioning in the Sea of Marmara pull-apart: A clue to propagation processes of the North Anatolian fault?, *Terra Nova*, *14*, 80–86.

Beresnev, I. A., and G. M. Atkinson (1997), Modeling finite-fault radiation from the ω^n spectrum, *Bull. Seismol. Soc. Am.*, *87*, 67–84.

Boore, D. M., and W.B. Joyner (1997), Site amplifications for generic rock studies, *Bull. Seismol. Soc. Am.*, *87*, 327–341.

Böse, M. (2006), Earthquake early warning for Istanbul using artificial neural networks, Ph.D. thesis, 181 pp., Karlsruhe University, Karlsruhe, Germany.

Böse, M., E. Hauksson, K. Solanki, H. Kanamori, and T. H. Heaton (2009), Real-time testing of the on-site warning algorithm in southern California and its performance during the July 29, 2008 Mw 5.4 Chino Hills earthquake, *Geophys. Res. Lett.*, *36*, L00B03, doi:10.1029/2008GL036366.

Böse, M., F. Wenzel, and M. Erdik (2008), PreSEIS: A neural network-based approach to earthquake early warning for finite faults, *Bull Seismol. Soc. Am.*, *98*, 366–382, doi:10.1785/0120070002.

Carroll, D. L. (1996), Genetic algorithms and optimizing chemical oxygen-iodine lasers, in *Developments in Theoretical and Applied Mechanics*, *Vol.* XVIII, edited by H. B. Wilson et al., School of Engineering, The University of Alabama, pp. 411–424.

Cua, G., M. Fischer, T. Heaton, and S. Wiemer (2009), Real-time performance of the Virtual Seismologist earthquake early warning algorithm in Southern California, *Seismol. Res. Lett.*, *80*(5), pp. 740–747.

Erdik, M., Y. Fahjan, O. Ozel, H. Alcik, A. Mert, and M. Gul (2003), Istanbul earthquake rapid response and early warning system, *Bull Earthq. Eng.*, *1*, 157–163.

Espinosa-Aranda, J. M., A. Jimenez, G. Ibarrola, F. Alcantar, A. Aguilar, M. Inostroza, and S. Maldonado (1995), Mexico City seismic alert system, *Seismol. Res. Lett.*, *66*, 42–53.

Goldberg, D. (1989), *Genetic algorithms in search for optimization and machine learning*, Addison-Wesley, New York.

Haupt, R. L., and S. E. Haupt (1998), *Practical Genetic Algorithms*, Wiley-Interscience, New York.

Hubert-Ferrari, A., A. Barka, E. Jacques, S. S. Nalbant, B. Meyer, R. Armijo, P. Tapponnier, and G. C. P. King (2000), Seismic hazard in the Sea of Marmara following the Izmit earthquake, *Nature*, *404*, 269–272.

Kamigaichi, O., M. Saito, K. Doi, T. Matsumori, S. Tsukada, K. Takeda, T. Shimoyama, K. Nakamura, M. Kiyomoto, and Y. Watanbe (2009), Earthquake early warning in Japan: Warning the general public and future prospects, *Seismol. Res. Lett.*, *80*, 717–726.

Kanamori, H. (2005), Real-time seismology and earthquake damage mitigation, *Annu. Rev. Earth Planet. Sci.*, *33*, 195–124, doi:10.1146/annurev.earth.33.092203.122626.

Krishnakumar, K. (1989), Micro-Genetic Algorithms for stationary and non-stationary function optimization, in *Proceedings of SPIE: Intelligent Control and Adaptive Systems*, Vol. 1196, Philadelphia, PA, pp. 289–296.

Le Pichon, X., N. Chamot-Rooke, C. Rangin, and A. M. C. Sengor (2002), The North Anatolian fault in the Sea of Marmara, *J. Geophys. Res.*, *108*(B4), 2179, doi:10.1029/2002JB001862.

Nakamura, Y. (1988), On the urgent earthquake detection and alarm system (UrEDAS), in *Proc. of the 9th World Conference on Earthquake Engineering VII*, 673–678.

Olson, E., and R. M. Allen (2005), The deterministic nature of earthquake rupture, *Nature*, *438*, 212–215.

Parolai, S., A. Ansal, A. Kurtulus, A. Strollo, R. Wang, and J. Zschau (2009), The Ataköy vertical array (Turkey): Insights into seismic wave propagation in the shallow-most crustal layers by waveform deconvolution, *Geophys. J. Int.*, *178*, 1649–1662, doi:10.1111/j.1365-246X.2009.04257.x.

Parsons, T. (2004), Recalculated probability of $M \geq 7$ earthquakes beneath the Sea of Marmara, Turkey, *J. Geophys. Res.*, *109*, B05304, doi:10.1029/2003JB002667.

Petersen, M. D., A. D. Frankel, S. C. Harmsen, C. S. Mueller, K. M. Haller, R. L. Wheeler, R. L. Wesson, Y. Zeng, O. S. Boyd, D. M. Perkins, N. Luco, E. H. Field, C. J. Wills, and K. S. Rukstales (2008), Documentation for the 2008 update of the United States national seismic hazard maps, *U. S. Geological Survey Open File Rep. 2008–1128*, 61 pp.

Somerville, P., K. Irikura, R. Graves, S. Sawada, D. Wald, N. Abrahamson, Y. Iwasaki, T. Kagawa, N. Smith, and A. Kowada (1999), Characterizing crustal earthquake slip models for the prediction of strong ground motion, *Seismol. Res. Lett.*, *70*, 59–80.

Tarantola, A. (2005), Inverse problem theory and methods for model parameter estimation, *SIAM: Soc. Indust. Appl. Math*, 352 pp.

Wald, D. J., and T. I. Allen (2007), Topographic slope as a proxy for seismic site conditions and amplification, *Bull. Seismol. Soc. Am.*, *97*, 1379–1395.

Wald, D. J., L. Wald, B. Worden, and J. Goltz (2003), ShakeMap: A tool for earthquake response, *U. S. Geological Survey Fact Sheet 087-03*.

Zollo, A., G. Iannacone, M. Lancieri, L. Cantore, V. Convertito, A. Emolo, G. Festa, F. Gallovic, M. Vassallo, C. Martino, C. Satriano, and P. Gasparini (2009), Earthquake early warning system in southern Italy: Methodologies and performance evaluation, *Geophys. Res. Lett.*, *36*, L00B07, doi:10.1029/2008GL036689.

M. Böse, Seismological Laboratory, California Institute of Technology, 1200 East California Boulevard, Pasadena, CA 91125, USA.

M. Erdik, Kandilli Observatory and Earthquake Research Institute, Department of Earthquake Engineering, Bogazici University, 81220 Cengelköy, Istanbul, Turkey.

N. Köhler, Swiss Re Europe S.A., Niederlassung Deutschland, Dieselstr. 11, 85774 Unterföhring, Germany.

A. Oth, European Center for Geodynamics and Seismology, 19 rue Josy Welter, L-7256 Walferdange, Grand-Duchy of Luxembourg. (adrien.oth@ecgs.lu)

F. Wenzel, Geophysical Institute, Karlsruhe Institute of Technology (KIT), Hertzstr. 16, 76187 Karlsruhe, Germany.